The Astronomical Journal, 125:2783–2808, 2003 June

NEW OPTICAL AND NEAR-INFRARED SURFACE BRIGHTNESS FLUCTUATION MODELS: A PRIMARY DISTANCE INDICATOR RANGING FROM GLOBULAR CLUSTERS TO DISTANT GALAXIES?

M. Cantiello,[1,2] G. Raimondo,[1,3] E. Brocato,[1,4] and M. Capaccioli[5,6]
Received 2002 September 25; accepted 2003 March 13

ABSTRACT

We present new theoretical models for surface brightness fluctuations (SBFs) both for optical and near-infrared bands in standard ground-based and *Hubble Space Telescope* filter systems. Simple stellar population simulations are adopted. Models cover the age and metallicity ranges from 5 to 15 Gyr and from $Z = 0.0001$ to $Z = 0.04$, respectively. Effects due to variation of the initial mass function and the stellar color-temperature relation are explored. Particular attention is devoted to very bright stars in the color-magnitude diagram and to investigating the effects of mass loss along the red giant branch (RGB) and the asymptotic giant branch (AGB). It is found that *U*- and *B*-band SBF amplitudes are powerful diagnostics for the morphology of the horizontal branch and the post-AGB star population. We point out that a careful treatment of the mass-loss process along the RGB and AGB is fundamental to determining reliable SBF evaluations. The SBF measurements are used to place robust constraints on the evolution of AGB stars, suggesting that the mass-loss activity of AGB stars should be twice as efficient as that of RGB stars. Our models are able to reproduce the absolute SBF magnitudes of Galactic globular clusters and of galaxies and their integrated colors. New calibrations of absolute SBF magnitude in *V*, *R*, *I*, and *K* photometric filters are provided, which appear reliable enough to directly gauge distances, bypassing other distance indicators. The SBF technique is also used as a stellar population tracer to derive the age and metallicity of a selected sample of galaxies of known distances. Finally, *SBF color* versus *integrated color* diagrams are proposed as particularly useful in removing the well-known age-metallicity degeneracy affecting our knowledge of remote stellar systems.

Key words: distance scale — galaxies: distances and redshifts — galaxies: stellar content — globular clusters: general

1. INTRODUCTION

Our understanding of external galaxies, which are milestones in cosmological evolution, relies on our ability to gauge their distances, ages, and chemical compositions. Surface brightness fluctuations (SBFs) are recognized as a powerful tool for providing accurate answers to all these challenges (Tonry, Ajhar, & Luppino 1990, hereafter TAL90; Buzzoni 1993, hereafter B93; Worthey 1993, hereafter W93; Brocato, Capaccioli, & Condelli 1998; Blakeslee, Ajhar, & Tonry 1999; Liu, Charlot, & Graham 2000, hereafter LCG00; Blakeslee, Vazdekis, & Ajhar 2001, hereafter BVA01). Since the first attempt at using the SBF in galaxies to estimate cosmic distances (Tonry & Schneider 1988, hereafter TS88), a major observational effort has been made to improve the accuracy of the method (TAL90; Luppino & Tonry 1993; Lorenz et al. 1993; Tonry et al. 1997, hereafter TBAD97). As a matter of fact, the typical uncertainties on the distances derived via SBFs are on the order of 10% or less (Mei, Quinn, & Silva 2001). Moreover, SBFs work well over a wide range of distances, from Local Group objects out to galaxy clusters such as Virgo, Fornax, and even Coma. Recently, Jensen et al. (2001) succeeded in reaching galaxies at 150 Mpc ($H_0 = 75$ km s^{-1} Mpc^{-1}) using near-infrared (NIR) *Hubble Space Telescope* (*HST*) data.

The largest SBF database available so far is that of Tonry et al. (2001, hereafter T01, and references therein). They measured the *I*-band SBF of nearly 300 galaxies and were able to empirically calibrate the absolute SBF amplitude in this same band with reference to Cepheid-derived distances. Calibrations in other bands have been provided by BVA01 in *V*, in the *K* band by Liu, Graham, & Charlot (2002, hereafter LGC02), and in the F160W band by Jensen et al. (2003). Relying on measurements of dwarf elliptical galaxies (e.g., Jerjen, Freeman, & Binggeli 1998; Jerjen, Binggeli, & Freeman 2000), Jerjen et al. (2001) calibrated the *R*-band SBF absolute magnitude versus the galaxy $(B-R)_0$ color.

This paper provides a new approach to deriving SBFs for simple stellar populations (SSPs; see Renzini & Buzzoni 1986). Our first goal is to revise the theoretical calibrations of the absolute magnitudes of the optical and NIR SBFs. The reason is that empirical calibrations rest on some other indicators, thus confining SBFs to the role of at least secondary distance indicators (SBF errors sum to the uncertainties of the primary distance indicators). Such a limitation may be removed by theoretical SBF models that, by providing *absolute galaxy SBF magnitude* versus *integrated color* relations for several different filters, set the SBF method into

[1] Osservatorio Astronomico di Collurania, INAF, via M. Maggini, I-64100 Teramo, Italy; brocato@te.astro.it, cantiello@te.astro.it, raimondo@te.astro.it.
[2] Dipartimento di Fisica "E.R. Caianiello," Università di Salerno; and Sezione di Napoli, Gruppo Collegato di Salerno, INFN, via S. Allende, I-4081 Baronissi, Salerno, Italy.
[3] Dipartimento di Fisica, Università La Sapienza, Piazzale Aldo Moro 2, I-00185 Roma, Italy.
[4] Istituto Nazionale di Fisica Nucleare, LNGS, L'Aquila, Italy.
[5] Dipartimento di Scienze Fisiche, Università di Napoli Federico II, Complesso Monte S. Angelo, via Cintia, I-80126 Napoli, Italy; capaccioli@na.astro.it
[6] Osservatorio Astronomico di Capodimonte, INAF, via Moiariello 16, I-80131 Napoli, Italy.

the class of *primary distance indicators*. Of course, one needs a high degree of reliability for the adopted theoretical framework.

A second goal is to probe the capability of our SBF models in analyzing the stellar content of star clusters and galaxies as a complementary tool to the *classical* method based on integrated magnitudes and colors. Unfortunately, disentangling the information on the main physical quantities that define the dominant stellar populations, the formation, and the evolution processes in elliptical and spiral galaxies from their integrated broadband colors and spectral features still remains an intriguing problem (Brocato et al. 1990; Weiss, Peletier, & Matteucci 1995; Bressan, Chiosi, & Tantalo 1996; Kobayashi & Arimoto 1999; Trager et al. 2000, hereafter TFWG00). For instance, even in the simple case of elliptical galaxies, age works in masking possible metallicity effects (Renzini & Buzzoni 1986; Worthey 1994). Since SBFs are generated by the Poissonian fluctuations of the stellar counts in each pixel of a galaxy image, they have a well-understood physical origin (dictated by the properties of the stellar population from which they originate). The amplitude of these fluctuations is determined by the age, chemical composition, and distribution of the evolving stars in the proper evolutionary phases. Thus, theoretical SBF colors and magnitudes are expected to provide a diagnostic of the stellar content of galaxies, which is useful in decoupling age from metallicity (LCG00; BVA01).

So far, only a handful of theoretical works on SBF modeling are available (W93; B93; LCG00; BVA01; Mei et al. 2001). Despite these impressive results, models based on different ingredients (stellar evolutionary tracks, temperature-color transformations) and detailed assumptions (horizontal branch morphology, asymptotic giant branch evolution, mass loss, etc.) are still needed in order to compare the various theoretical expectations and thus improve the reliability of the theoretical framework. An enlightening example of the present situation is offered by Figure 5 of LGC02, clearly showing that the inferred ages and metallicities depend on the choice of models.

The presentation of our work is organized as follows: The basis of the model is described in § 2, where we also present absolute magnitudes and colors for the optical and NIR ground-based and *HST* filters under different assumptions for the chemical composition and age. Section 3 reports on a comparison between our SBF predictions and those of other authors. The effects of the initial mass function (IMF) and the contribution of stars in late evolutionary phases are explored in § 4, together with a discussion on the impact of using different color-temperature libraries. After testing our SBF models as distance indicators on Galactic globular clusters (GGCs) and galaxies, in § 5 they are applied to derive the population parameters of some galaxies. Theoretical calibrations are presented in § 6. The main results are summarized in § 7.

2. SBF SYNTHETIC MODEL

Our SBF model is based on the stellar population synthesis code described and tested observationally in Brocato et al. (1999, 2000). This code is optimized to reproduce both the observed distribution of stars in the color-magnitude diagrams (CMDs) and the integrated properties (color and spectral indices, energy distribution, etc.) of GGCs and galaxies. Here we report the main ingredients used in the present version of the code, referring to the quoted papers for details on the theoretical background.

All the computations refer to simple stellar populations, i.e., single-burst stellar systems with homogeneous chemical composition, and an IMF to be randomly populated by our model machinery (Appendix). Those models computed by assuming a bimodal Scalo-like IMF in the mass range 0.1–1.5 $M_{\odot}$ will be called reference models hereafter.

The database of stellar evolutionary tracks is from the Teramo-Pisa-Rome group, based on the evolutionary stellar code FRANEC (Cassisi et al. 1998 and references therein). Here we include tracks with metallicity ranging from $1/200\ Z_{\odot}$ to supersolar metallicity, $2\ Z_{\odot}$ (Castellani, Chieffi, & Pulone 1991; Castellani, Chieffi, & Straniero 1992; Bono et al. 1997b, 1997a). These sets of tracks cover all the major evolutionary phases: main sequence (MS), subgiant branch (SGB), red giant branch (RGB), He-burning phase (horizontal branch [HB]) and asymptotic giant branch (AGB). The latest stages, which are crucial for SBF calculations, have been treated with special care; they extend to post-AGB (PAGB) and white dwarf (WD) sequences when needed.

In each reference model, mass loss along the RGB and AGB is taken into account following the prescriptions of Reimers (1975). In particular, along the RGB we adopt $\eta = 0.4$, which is able to reproduce the typical HB star distributions and the integrated colors in globular clusters (Renzini & Fusi Pecci 1988; Brocato et al. 2000, hereafter BCPR00). A slightly higher value is taken for stars in the upper part of the AGB ($\eta_{\rm AGB} = 0.8$; see § 4.2.2), which reproduces the observed amount of mass loss of very bright stars (Le Bertre et al. 2001).

The magnitudes of the stars are derived assuming the bolometric corrections and colors of Lejeune, Cuisinier, & Buser (1997, hereafter LCB97) for the standard Johnson-Cousins *UBVRIJHK* photometric system. We also provide SBF amplitudes for a set of *HST* WFPC2 and NICMOS filters covering almost the same range of wavelengths (namely, F439W, F555W, F814W, F110W, F160W, and F222M), adopting the transformation tables of Origlia & Leitherer (2000, hereafter OL00). The effects of other transformation recipes, resting on different assumptions, will be discussed in § 4.3. As an example of the color-magnitude diagrams of the SSP under investigation, we plot in Figure 1 a sample of CMDs for a fixed age, $t = 15$ Gyr, and for three chemical compositions, $Z = 0.001$, 0.01, and 0.02.

The present procedure for deriving the SBFs differs from the "usual" one, which is based on the ratio of the second to the first moment of the luminosity function (TS88; W93; Worthey 1994; LCG00; BVA01). Our method is briefly outlined here; a detailed description and a discussion are reported in the Appendix and in Cantiello (2001).

By a Monte Carlo random method, we compute an SSP model with a fixed number of stars $N_{\rm star}$ for a given set of stellar population parameters: age, chemical composition, IMF, etc. This provides an integrated flux (F_X) within each specific filter X. The same set of parameters is used to compute $N_{\rm sim}$ independent simulations. The corresponding SBFs are explicitly calculated as

$$\bar{F}_X = \langle F_X - \langle F_X \rangle^2 \rangle / \langle F_X \rangle \ , \qquad (1)$$

where $\bar{F}_X$ is the flux fluctuation from which we derive the SBF amplitude $\bar{M}_X$.

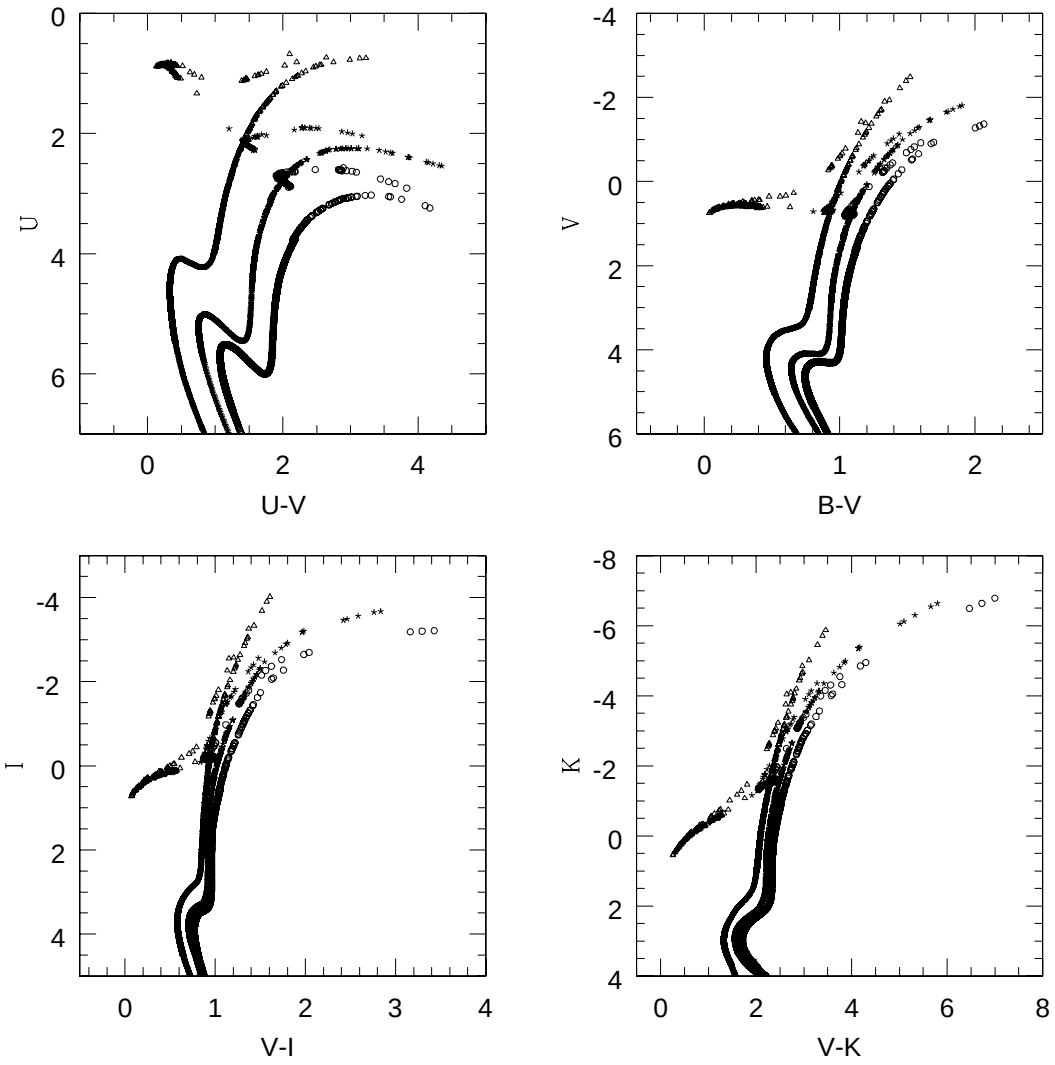

FIG. 1.—Simulated color-magnitude diagrams for a fixed age ($t = 15$ Gyr) and for three values of metallicity: $Z = 0.001$ (*triangles*), 0.01 (*stars*), and 0.02 (*circles*).

To match the typical number of stars per pixel in real observations $N_{\rm star}$ is chosen to be $\simeq 10^5$ (e.g., B93). By increasing $N_{\rm sim}$ (to a maximum of 10^5 experiments), the "fluctuations" of $\bar{M}_X$ tend to vanish, i.e., $\bar{M}_X$ tends to an asymptotic value. As an example, Figure 2 shows the value of the *I*-band SBF amplitude ($\bar{M}_I$) versus $N_{\rm sim}$ for a model with $Z = 0.02$, $Y = 0.289$, and $t = 15$ Gyr. For small $N_{\rm sim}$ (e.g., $N_{\rm sim} \lesssim 500$), $\bar{M}_I$ oscillates strongly. For $N_{\rm sim} > 1000$ simulations, $\bar{M}_I$ approaches the asymptotic value $\bar{M}_I^{\rm asym} \simeq -1.47$ mag and keeps well within the best observational accuracy of SBF measurements ($\sim$0.05; T01), i.e., $|\bar{M}_I - \bar{M}_I^{\rm asym}| \lesssim 0.05$. By repeating the same procedure for different sets of the parameters of stellar populations and for different filters, we found that $N_{\rm sim}^* = 5000$ is appropriate to all the photometric bands used here for the adopted $N_{\rm star} \simeq 10^5$.

2.1. *SBF versus Chemical Composition and Age*

In order to cover the typical chemical compositions and ages of both GGCs and galaxies, we computed the SBF absolute magnitudes for the following set of chemical compositions: ($Z = 0.0001$, $Y = 0.23$); ($Z = 0.001$, $Y = 0.23$); ($Z = 0.01$, $Y = 0.255$); ($Z = 0.02$, $Y = 0.289$); and ($Z = 0.04$, $Y = 0.34$). The values for the ages are $t = 5$, 9, 11, 13, and 15 Gyr. The resulting SBFs are listed in Tables 1A and 1B, for ground-based and *HST* filters, respectively. The complete output of the models (CMDs, integrated colors, and SBF amplitudes) are available on the Web.[7]

Figure 3 reports the SBF predictions as a function of metallicity. We consider two ages, 15 and 5 Gyr, and both sets of filters (Fig. 3*a* refers to ground-based, Fig. 3*b* to *HST* filters). In the optical range all the SBF amplitudes become fainter with increasing metallicity, while the opposite trend is shown by NIR bands. This behavior does not depend on age, at least in the range investigated in this paper. Moreover, it supports the conclusion by W93 of the possible existence of an ideal filter centered at $\sim$1 μm that is expected to be independent of metallicity.

For $Z \lesssim 0.01$ the least sensitive band is *I*; this means that $\bar{M}_I$ is an excellent distance indicator for metal-poor old

[7] See http://www.te.astro.it/osservatorio/personale/brocato/brocato.html

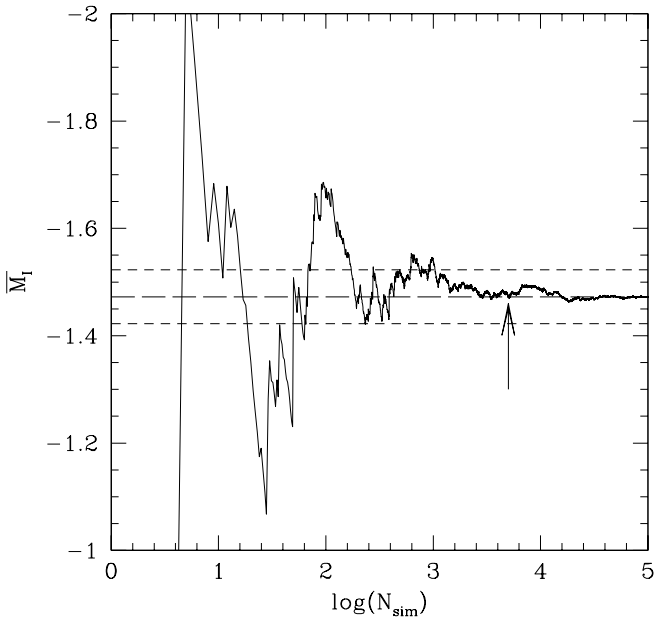

FIG. 2.—SBF amplitude $\bar{M}_I$ as a function of the number of Monte Carlo cycles. For $N_{\rm sim} > 1000$, $\bar{M}_I$ varies around the asymptotic value (the permitted region is delimited by the dashed lines) by an amount well within the typical observational uncertainties ($\sim$0.05). The arrow indicates the value $N^*_{\rm sim} = 5000$ adopted in our calculations (see text).

stellar systems. At higher metallicities ($Z \gtrsim 0.01$) the slope of the $\bar{M}_X$ versus Z relation increases for all SBF amplitudes and is similar for all bands ($BVRI$) except for U. In general, $\bar{M}_U$ has quite a different behavior in the whole range of metallicity, varying by $\sim$3.2 mag because of the strong decrease of the U mean luminosity of the brightest stars in the population as the metallicity increases (Fig. 1). Although ruling out $\bar{M}_U$ as a reliable distance indicator, this high sensitivity makes it an excellent population tracer. Unfortunately, no SBF measurements are available in the U filter so far.

The predicted small variations of J, H, and K bands at $Z \gtrsim 0.01$, coupled with high luminosity, supports the increasing number of SBF measurements in these bands. The SBF amplitudes computed for the *HST* filters (Fig. 3*b*) show a behavior quite similar to the corresponding ground-based filters.

The next step is to understand the effects of variations in the age of the stellar population on the SBF amplitudes. The results of our computations for models of age $t = 5$, 9, 11, 13, and 15 Gyr are plotted in Figure 4 for both a metal-rich ($Z = 0.02$) and a metal-poor ($Z = 0.0001$) stellar system. In general, the sensitivity to age grows from U to I, with changes remaining below $\sim$0.4 mag. The J, H, and K bands are more sensitive; SBF amplitudes increase by about 0.7 mag from 5 to 15 Gyr, in agreement with BVA01 and LCG00. However, for stellar populations with ages in the range under consideration, J, H, and K SBFs are strictly dependent on the adopted treatment of the brightest evolutionary phases (thermal pulses, mass-loss processes, etc.), as we show in § 4.2.

Finally we note that the SBF amplitudes for old stellar populations are much more sensitive to metallicity changes than to age, particularly at optical wavelengths. A similar conclusion, even with slightly different absolute SBF values, has been reached by other authors (B93; LCG00; BVA01), who adopt different approaches and ingredients to derive population synthesis models. In this sense, this result may be regarded as theoretically well established; i.e., it does not depend on the adopted stellar population models.

TABLE 1A

SURFACE BRIGHTNESS FLUCTUATIONS FOR THE REFERENCE MODELS: GROUND-BASED FILTERS

Z	Y	Age	$\bar{M}_U$	$\bar{M}_B$	$\bar{M}_V$	$\bar{M}_R$	$\bar{M}_I$	$\bar{M}_J$	$\bar{M}_H$	$\bar{M}_K$	$V-I$
0.0001	0.23	5	1.711	0.934	−0.776	−1.771	−2.690	−3.719	−4.456	−4.658	0.776
		9	1.527	0.759	−0.815	−1.738	−2.592	−3.564	−4.266	−4.457	0.855
		11	1.552	0.774	−0.719	−1.596	−2.409	−3.355	−4.035	−4.218	0.858
		13	1.577	0.827	−0.636	−1.490	−2.283	−3.216	−3.884	−4.062	0.871
		15	1.534	0.811	−0.610	−1.425	−2.185	−3.102	−3.752	−3.923	0.891
0.001	0.23	5	2.426	1.176	−0.685	−1.776	−2.817	−4.009	−4.949	−5.184	0.913
		9	2.304	1.131	−0.571	−1.548	−2.464	−3.564	−4.441	−4.650	0.965
		11	2.367	1.198	−0.474	−1.424	−2.306	−3.375	−4.235	−4.434	0.977
		13	2.183	1.141	−0.478	−1.404	−2.260	−3.312	−4.158	−4.349	0.980
		15	2.008	1.080	−0.425	−1.331	−2.174	−3.215	−4.057	−4.244	0.959
0.01	0.255	5	3.476	1.801	0.055	−1.037	−2.495	−4.348	−5.488	−5.839	1.075
		9	3.386	1.875	0.237	−0.797	−2.164	−4.027	−5.153	−5.542	1.114
		11	3.388	1.887	0.256	−0.775	−2.126	−3.868	−4.982	−5.339	1.130
		13	3.351	1.902	0.283	−0.758	−2.104	−3.728	−4.816	−5.152	1.151
		15	3.324	1.927	0.332	−0.697	−2.011	−3.644	−4.732	−5.082	1.167
0.02	0.289	5	4.124	2.247	0.528	−0.489	−1.918	−4.518	−5.656	−6.145	1.112
		9	4.230	2.352	0.702	−0.270	−1.671	−4.064	−5.190	−5.633	1.174
		11	4.169	2.325	0.710	−0.238	−1.612	−4.025	−5.150	−5.600	1.196
		13	4.111	2.344	0.759	−0.173	−1.526	−3.883	−5.010	−5.447	1.211
		15	4.085	2.353	0.781	−0.152	−1.513	−3.846	−4.974	−5.402	1.229
0.04	0.34	5	4.796	2.715	0.987	0.013	−1.411	−4.554	−5.654	−6.203	1.188
		9	4.792	2.763	1.116	0.193	−1.121	−4.120	−5.241	−5.770	1.249
		11	4.797	2.769	1.140	0.230	−1.045	−3.984	−5.111	−5.630	1.271
		13	4.779	2.804	1.198	0.299	−0.980	−3.948	−5.083	−5.600	1.288
		15	4.740	2.786	1.198	0.306	−0.960	−3.882	−5.012	−5.522	1.304

TABLE 1B

SURFACE BRIGHTNESS FLUCTUATIONS FOR THE REFERENCE MODELS: *HST* FILTERS

Z	Y	Age	$\bar{M}_{F439W}$	$\bar{M}_{F555W}$	$\bar{M}_{F814W}$	$\bar{M}_{F110W}$	$\bar{M}_{F160W}$	$\bar{M}_{F222M}$	$V-I$
0.0001	0.23	5	1.141	−0.794	−2.752	−3.442	−4.414	−4.566	0.776
		9	0.936	−0.834	−2.654	−3.302	−4.228	−4.370	0.855
		11	0.933	−0.735	−2.471	−3.099	−3.999	−4.133	0.858
		13	0.981	−0.650	−2.345	−2.963	−3.849	−3.978	0.871
		15	0.965	−0.623	−2.247	−2.853	−3.720	−3.842	0.891
0.001	0.23	5	1.410	−0.696	−2.897	−3.720	−4.873	−5.088	0.913
		9	1.339	−0.580	−2.541	−3.287	−4.374	−4.560	0.965
		11	1.402	−0.482	−2.382	−3.103	−4.170	−4.346	0.977
		13	1.331	−0.486	−2.336	−3.041	−4.095	−4.263	0.980
		15	1.233	−0.433	−2.249	−2.946	−3.995	−4.159	0.959
0.01	0.255	5	2.095	0.103	−2.625	−4.073	−5.394	−5.788	1.075
		9	2.117	0.240	−2.329	−3.738	−5.055	−5.455	1.114
		11	2.136	0.272	−2.272	−3.596	−4.882	−5.252	1.130
		13	2.161	0.327	−2.192	−3.472	−4.747	−5.097	1.151
		15	2.176	0.366	−2.120	−3.381	−4.644	−4.994	1.167
0.02	0.289	5	2.466	0.496	−2.246	−4.583	−5.605	−6.024	1.112
		9	2.567	0.675	−1.937	−3.737	−5.120	−5.515	1.174
		11	2.534	0.682	−1.890	−3.700	−5.081	−5.478	1.196
		13	2.547	0.733	−1.789	−3.564	−4.936	−5.327	1.211
		15	2.555	0.753	−1.770	−3.531	−4.897	−5.285	1.229
0.04	0.34	5	2.890	0.944	−1.791	−4.202	−5.741	−6.251	1.188
		9	2.930	1.077	−1.516	−3.779	−5.272	−5.756	1.249
		11	2.935	1.104	−1.437	−3.647	−5.120	−5.591	1.271
		13	2.967	1.163	−1.395	−3.613	−5.079	−5.545	1.288
		15	2.947	1.163	−1.368	−3.550	−5.005	−5.465	1.304

3. COMPARISONS WITH OTHER MODELS

We next compare our work with the models of BVA01 and LGC02. Since the grids of ages and metallicities do not match, we select values that are as similar as possible for the comparison. We restrict the discussion to populations of fixed age ($t \sim 15$ Gyr), and to V, I, and F160W photometric bands. Figure 5 plots the SBF predictions versus $(V-I)_0$ (*right*) and [Fe/H] (*left*) for single-burst stellar population models.

Despite the very different theoretical framework, the general trends of the SBF amplitudes versus both metallicity

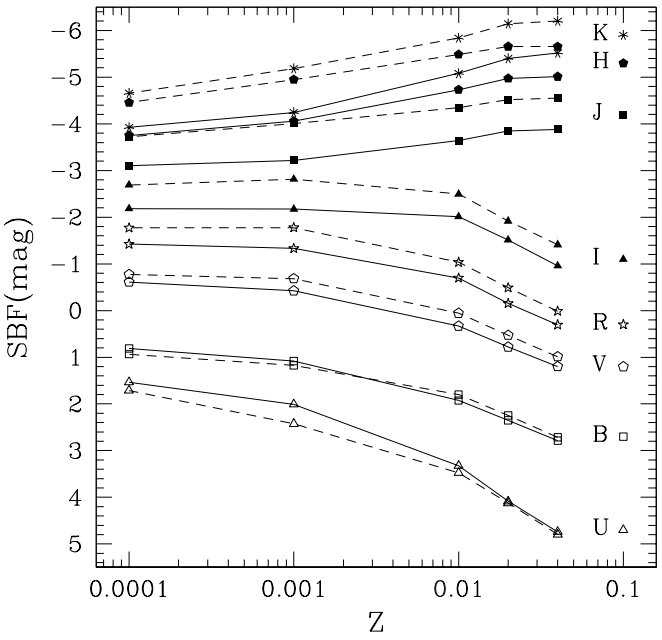

FIG. 3*a*

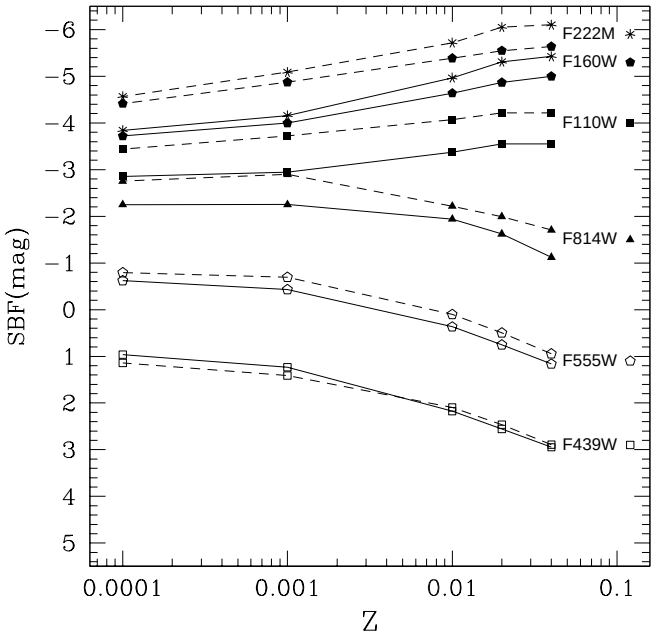

FIG. 3*b*

FIG. 3.—(*a*) Predicted SBF absolute magnitudes within *UBVRIJHK* ground-based filters for reference models aged 15 Gyr (*solid lines*) and 5 Gyr (*dashed lines*) vs. metal content. LCB97 transformations were adopted. The selected passbands are marked with different symbols, as labeled. (*b*) Same as (*a*), but for *HST* filters. In this case we adopt OL00 transformations.

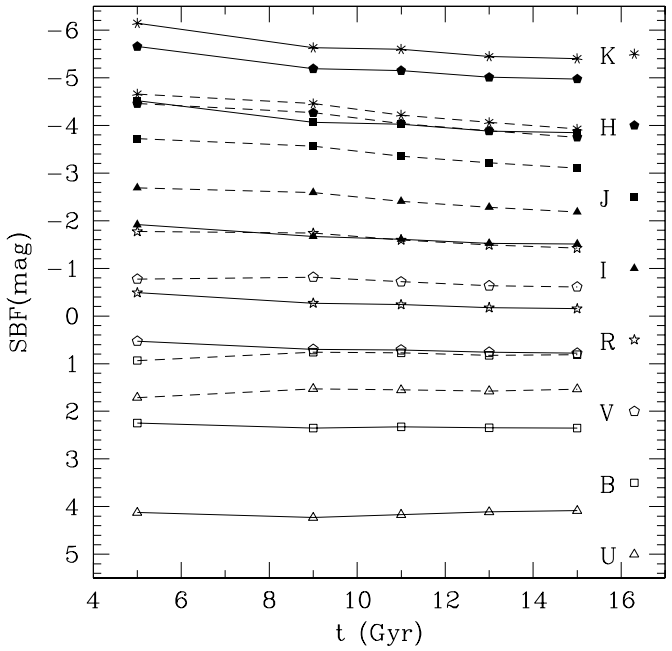

FIG. 4.—Predicted SBF absolute magnitudes within *UBVRIJHK* filters for reference models vs. age of the stellar population ($Z = 0.02$, *solid lines*; $Z = 0.0001$, *dashed lines*). The selected passbands are marked with different symbols, as labeled.

and the integrated $(V-I)_0$ color are the same for all authors. However, for metallicity higher than solar, BVA01 and LGC02 predict fainter SBF amplitudes in the V and I bands (up to $\sim$0.5 mag), and a similar, but less relevant, difference appears in the F160W band.

The reasons for such a discrepancy are expected to be in the basic ingredients and in the transformation tables. Our models are based on a completely different evolutionary framework compared with BVA01 and LCG00, whose models rely on the Padua stellar evolution database, although they use two different compilations of isochrones (Bertelli et al. 1994 and Girardi et al. 2000, respectively) and different prescriptions for the AGB stars. Furthermore, we adopt a different approach to populating the brightest evolutionary phases (HB, AGB, and thermal pulse) as we show in the following sections. For an extensive discussion of the impact of evolutionary tracks and transformations tables on SBF expectations, the reader may refer to LCG00 and to our § 4.3.

We note that there is a substantial difference in the meaning of the two panels of Figure 5: [Fe/H] is an input parameter for all the models, so it is directly comparable, while the $(V-I)_0$ color is an output of each code, and thus it depends on the adopted evolutionary tracks, on the procedure in populating the isochrones, and so on. Obviously, it may vary from model to model even for the same input parameters.

4. ASSUMPTIONS OF THE REFERENCE MODELS

Starting from the reference models, in this section we investigate the sensitivity of SBFs to IMF, late evolutionary phases, and color-temperature relations.

4.1. *Initial Mass Function*

Usually, the mass spectrum of a stellar population is described by the simple power law proposed by Salpeter (1955) or by the bimodal (or higher) function of Scalo (1986 and thereafter). Indeed, a crude extrapolation of the Salpeter law to masses $M \lesssim 1\ M_\odot$ seems to fail, while the flattening and even possible declining behavior of the Scalo IMF appears more appropriate. For these reasons, in our reference calculations we have adopted a Scalo-like IMF. Nevertheless, the slope of this function at the lowest masses remains very uncertain (Reid 1998). In this section we evaluate the contribution to the SBFs by the lowest mass stars and what happens under significant changes in the slope of the IMF. Two different numerical experiments are performed on an old solar-metallicity SSP ($t = 15$ Gyr, $Z = 0.02$, $Y = 0.289$).

First, SBF amplitudes are computed for a set of models obtained by adopting an IMF starting from different low-mass limits, namely, $M_{\rm low} = 0.85$, 0.6, 0.4, and 0.1 $M_\odot$, by keeping the number of RGB stars constant (actually $\sim$100). For all these simulations we adopt a Salpeter-like slope ($x = 1.35$) in order to enhance the contribution of very low mass stars (Table 2).

The table shows that the SBF amplitudes increase with the mass limit $M_{\rm low}$, with the differences being fairly negligible or small in all cases but in the interval 0.6–0.85 $M_\odot$, whose upper limit is on the order of our turnoff mass ($M_{\rm TO}$; in the model quoted here $M_{\rm TO} \simeq 0.90\ M_\odot$). As a matter of fact, the ignorance of the upper part of the MS ($M_{\rm TO} - M \leq 0.25\ M_\odot$) leads to an underestimate of the total luminosity of the population, which is obviously relevant in computing SBFs because it represents the denominator of equation (1). On the contrary, to add MS stars with $M < 0.6\ M_\odot$ causes small variations of the SBFs, since the total luminosity of the stellar population does not change significantly. Note that this is true even though stars with $M < 0.6\ M_\odot$ represent nearly 90% of the total number of stars in the population. In conclusion, no matter how (within reason) the mass spectrum at $M < 0.6\ M_\odot$ is chosen, its contribution to the SBFs will not exceed 0.1 mag in the most sensitive band, K.

TABLE 2

SBF AMPLITUDES FOR DIFFERENT ASSUMPTIONS ON THE LOWEST MASS LIMIT $M_{\rm LOW}$ FOR A POPULATION MODEL WITH $t = 15$ GYR, $Z = 0.02$, AND $Y = 0.289$

$M_{\rm low}$	$\bar{M}_U$	$\bar{M}_B$	$\bar{M}_V$	$\bar{M}_R$	$\bar{M}_I$	$\bar{M}_J$	$\bar{M}_H$	$\bar{M}_K$
0.85	3.886	2.146	0.571	−0.374	−1.716	−3.914	−5.024	−5.425
0.60	4.106	2.361	0.775	−0.174	−1.534	−3.769	−4.896	−5.306
0.40	4.117	2.377	0.798	−0.142	−1.487	−3.717	−4.845	−5.255
0.10	4.112	2.385	0.811	−0.122	−1.451	−3.668	−4.798	−5.205

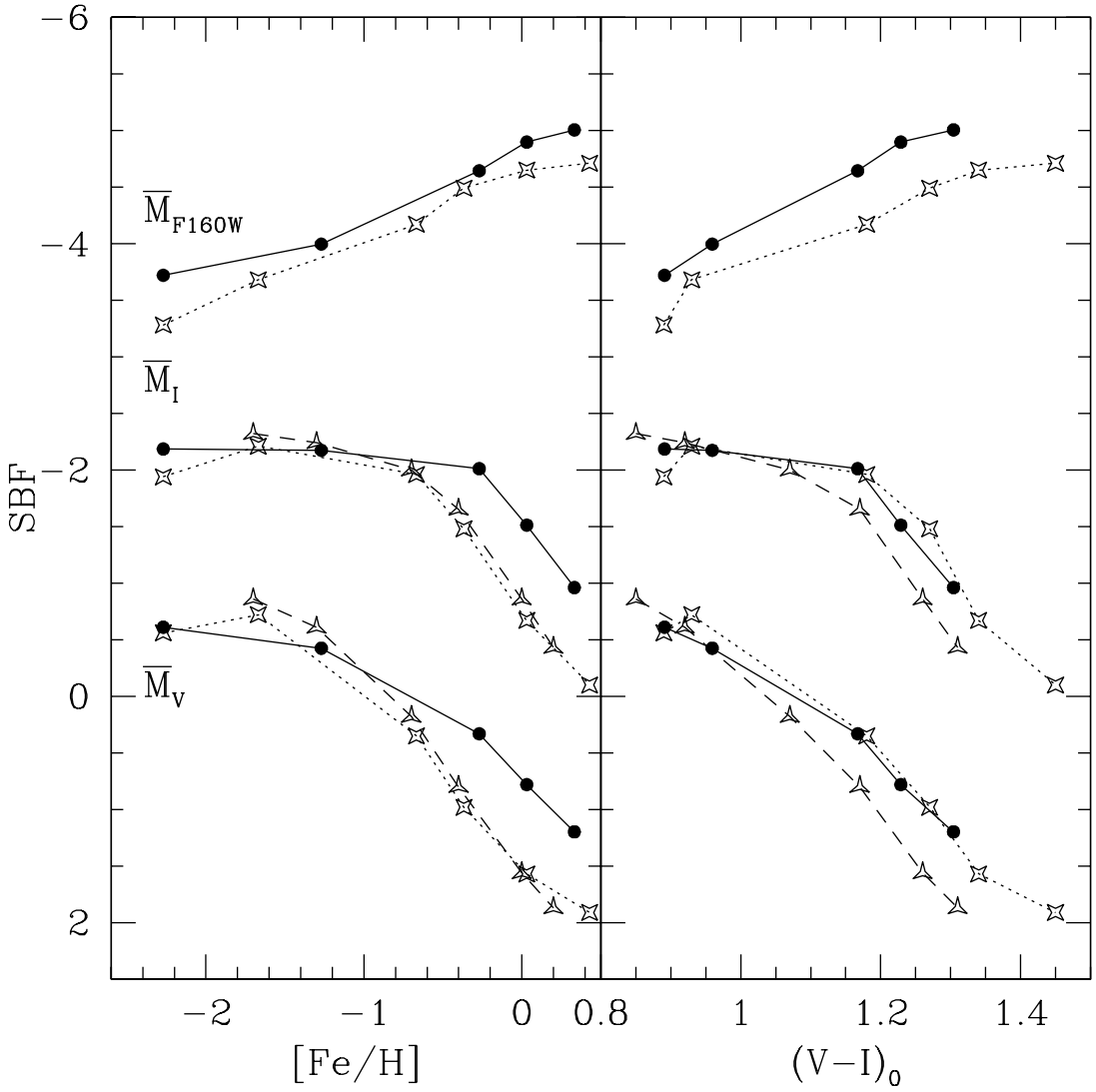

FIG. 5.—Comparison of SBF synthetic models with similar ages: LGC02 models with $t = 17$ Gyr (*dotted lines and four-pointed stars*); BVA01 models with $t = 15.8$ Gyr (*dashed lines and three-pointed stars*); present work models with $t = 15$ Gyr (*solid lines and filled circles*).

Second, the effect on the SBF values due to the IMF slope is explored by varying the exponent of the power law ($x = 0.35$, 1.35, and 2.35) for masses $M > 0.4\ M_\odot$ and assuming a flat distribution for masses $M < 0.4\ M_\odot$ (Table 3). Not surprisingly, the variations are rather small ($\Delta\bar{M}_X \lesssim 0.2$ mag); x mainly affects the number of MS stars, which in turn affect the predicted SBF amplitudes only slightly, as previously shown. However, an increased or decreased number of post-MS stars is foreseen if the exponent has a lower or higher value, respectively, than Salpeter's. Since the fluctuation rests mainly on the RGB stars, this explains why SBFs brighten with decreasing IMF exponents and vice versa.

We conclude that variations in the IMF slope, the contribution of low-mass stars to the SBF amplitude, or both, *although not negligible*, play a secondary role with respect to the quantities (and assumptions) affecting the post-MS evolution, such as the chemical composition and age of the populations. The result obtained with our new and fully independent code strengthens what was originally found by W93 and recently confirmed by other authors as well (e.g., BVA01).

TABLE 3

SBF AMPLITUDES FOR DIFFERENT IMF SLOPES x FOR A POPULATION MODEL WITH $t = 15$ GYR, $Z = 0.02$, AND $Y = 0.289$

x	$\bar{M}_U$	$\bar{M}_B$	$\bar{M}_V$	$\bar{M}_R$	$\bar{M}_I$	$\bar{M}_J$	$\bar{M}_H$	$\bar{M}_K$
0.35.....	4.029	2.300	0.733	−0.198	−1.552	−3.889	−5.011	−5.441
1.35.....	4.085	2.353	0.781	−0.153	−1.513	−3.846	−4.974	−5.402
2.35.....	4.170	2.441	0.873	−0.049	−1.385	−3.703	−4.838	−5.263

4.2. *SBFs versus Brightest Stars*

As stated above, the SBF signal is very sensitive to the properties of the most luminous stars of the stellar population, as it is the ratio of the second to the first moment of the stellar luminosity function. This requires that the SSP models reach a high level of accuracy in reproducing the post-MS evolution. Therefore, one of the aims in optimizing our code has been to fine-tune the stellar counts during the latest and fastest phases experienced by low-mass stars during their evolution (see also BCPR00). Below we discuss the expected SBF sensitivity to the very bright stars in post-MS evolutionary phases: HB morphology, thermal pulse (TP), and PAGB phases.

4.2.1. *Horizontal-Branch Morphology*

As is well known, the main parameter regulating the HB morphology of a generic stellar population is metallicity (Lee, Demarque, & Zinn 1987). If one considers just the effect of Z, the expected HB morphology is that of Figure 1: blue or intermediate for $Z \lesssim 0.001$, red when $Z > 0.004$. Thus, the distribution in color of low-mass stars during the central He-burning stage is expected to play a major role in predicting U and B SBFs (see also W93). This is particularly true for high metallicities, since the HB stars become brighter than the RGB tip (Fig. 1).

Although we do not discuss the nature of the second parameter (Freeman & Norris 1981), our models take into account the fact that the metallicity is not the only quantity that can affect the HB morphology. Here we adopt the HB morphology as directly produced by metallicity and by mass loss along the RGB (i.e., we use the mass loss to simulate the effect of the second parameter, whatever its real nature is). Along the same vein, one may recall that mass loss during the RGB evolution controls the actual total mass of the HB star and then affects its location in the CMD (Rood 1973). Moving from low to high values of mass loss, the total mass of the HB stars decreases; this fact implies, on average, higher temperatures and bluer colors. On the observational side, there are indications of mass-loss enhancement for increasing values of metallicity (e.g., Kudritzki, Pauldrach, & Puls 1987). On this basis, we investigated the importance of HB morphology on SBFs by simulating different amounts of mass-loss along the RGB, i.e., we changed η in the Reimers (1975) formula ($\eta = 0.2$, 0.4, 0.6, and 0.8) in computing a set of SSP models with a given metallicity ($Z = 0.01$, 0.02, and 0.04) and age ($t = 15$ Gyr).

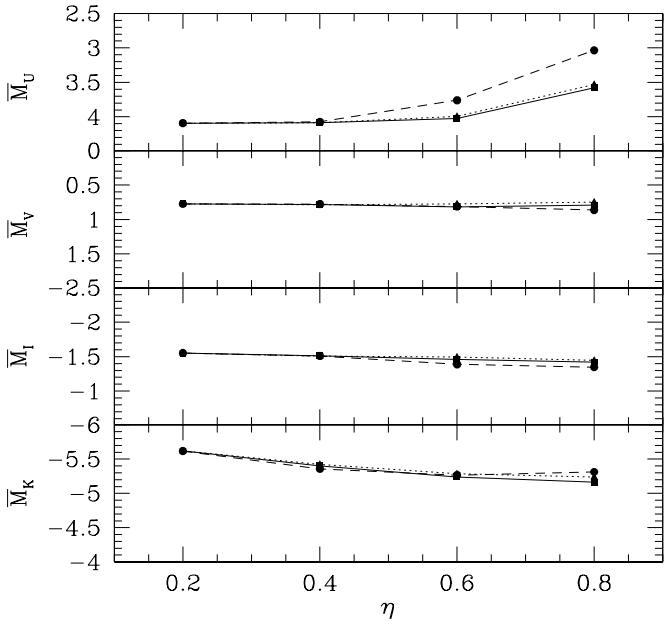

FIG. 6.—Effect of mass-loss variations along the RGB on *UVIK*-band SBF magnitudes. The mass loss is parameterized by the η-coefficient of the Reimers formula: $Z = 0.04$ (*dotted line*), $Z = 0.02$ (*solid line*), and $Z = 0.01$ (*dashed line*). All models refer to $t = 15$ Gyr populations. For graphical reasons, we shifted all nonsolar models to match the SBF values of the solar model with $\eta = 0.2$.

Table 4 summarizes the SBF values for all ground-based filters. The effects on *UVIK*-band SBF amplitudes are shown in Figure 6. The growth in luminosity of U-band SBFs and the constancy of the other optical bands confirms the above expectation. We note that the effect is more pronounced for $Z = 0.01$ ($\Delta\bar{M}_U \sim 1$ mag). For this metallicity, an enhancement of the mass loss on the RGB reduces the mass of the "forthcoming" HB stars by a quantity large enough to populate the blue side of the HB. The larger the mass loss, the larger the number of blue HB stars, and, consequently, the larger the U-band SBF amplitude. For higher metallicity systems, variations are still present but of smaller amplitude ($\Delta\bar{M}_U \sim 0.5$ mag), because the mass of the RGB stars for the selected age is so large that only red HB stars

TABLE 4

SBF AMPLITUDES FOR SIMPLE STELLAR POPULATIONS WITH AGE $t = 15$ GYR AND DIFFERENT VALUES OF REIMERS' COEFFICIENT η

Z	η	$\bar{M}_U$	$\bar{M}_B$	$\bar{M}_V$	$\bar{M}_R$	$\bar{M}_I$	$\bar{M}_J$	$\bar{M}_H$	$\bar{M}_K$	$V-I$
0.01	0.2	3.342	1.915	0.329	−0.682	−2.054	−3.853	−4.976	−5.341	1.173
	0.4	3.324	1.927	0.332	−0.697	−2.011	−3.644	−4.732	−5.082	1.167
	0.6	3.009	1.885	0.367	−0.623	−1.890	−3.542	−4.634	−4.990	1.148
	0.8	2.284	1.620	0.417	−0.540	−1.850	−3.563	−4.673	−5.036	1.078
0.02	0.2	4.092	2.345	0.774	−0.159	−1.552	−4.035	−5.163	−5.618	1.234
	0.4	4.085	2.353	0.781	−0.152	−1.513	−3.846	−4.974	−5.402	1.229
	0.6	4.023	2.375	0.818	−0.116	−1.459	−3.699	−4.827	−5.237	1.221
	0.8	3.578	2.273	0.791	−0.122	−1.418	−3.621	−4.756	−5.164	1.201
0.04	0.2	4.746	2.780	1.186	0.288	−1.004	−4.062	−5.192	−5.719	1.311
	0.4	4.740	2.786	1.198	0.306	−0.960	−3.882	−5.012	−5.522	1.304
	0.6	4.646	2.758	1.188	0.305	−0.945	−3.761	−4.889	−5.388	1.292
	0.8	4.186	2.638	1.160	0.307	−0.898	−3.696	−4.835	−5.338	1.260

are produced, even for the largest mass-loss rates considered here.

From Figure 6 it is also apparent the opposite behavior is shown by $\bar{M}_K$, which depends on the fact that, as η increases, the number of bright stars evolving on the AGB is smaller. Let us note here that an age of 15 Gyr was selected because models with younger ages provide a red clumpy HB morphology independent of any reasonable value of the η-parameter. This is because, by decreasing the age, the HB is populated by stars of increasing mass, which spend their He-burning phase on the red portion of the HB. Thus, no changes are expected in the SBFs. An unlikely value of $\eta \sim 2.0$ during the RGB phase would be needed to force the models to a blue HB morphology. However, this extremely high mass loss on the RGB would imply a similar (or larger) efficiency along the AGB. This means that the stars are expected to lose their hydrogen envelope and quickly move to the WD cooling sequence during the very early part of the AGB ascension (Castellani & Tornambé 1993). Such an improbable scenario leads to SBFs that are found to be fainter, particularly for the redder colors (up to 1 mag for the *K* band), when compared with models with more realistic assumptions for the RGB mass-loss efficiency.

The present results, even if they do not provide an exhaustive picture of the problem, give quantitative indications for the *U*- and *B*-band SBF variations as a function of the HB morphology. The effect of η on SBFs was also explored by B93, but those synthetic models always have a red clumpy HB morphology for populations with $Z > 0.001$. We conclude that changes in the HB morphology, as induced by reasonable assumptions for the mass loss along the RGB, have a negligible impact on SBFs, if one considers filters redder than *B*.

4.2.2. *Thermal Pulses*

Mass loss strongly affects the He exhaustion stages, too, and determines different scenarios for the evolution of stars leaving the HB, either to the TP phase or rapidly to a PAGB condition. According to the observations (e.g., Alard et al. 2001), mass loss becomes more and more efficient as the star climbs the AGB, until the ejection of the stellar envelope during the last superwind stages (Renzini 1981).

To extend our He-burning evolutionary tracks to the TP phase, we follow the prescriptions of Groenewegen & de Jong (1993), as in a previous paper (BCPR00). As cited above, our reference models simulate the mass-loss process along the AGB by adopting an enhanced Reimers coefficient η (namely, $\eta_{\rm AGB} = 0.8$). The corresponding mass lost by stars is in the range from 10^{-7} to 10^{-6} $M_{\odot}$ yr^{-1}, in fair agreement with observations of AGB stars (e.g., Le Bertre et al. 2001).

If the age of the population is fixed, an increase in the mass-loss rate is reflected in a decrease of the number of very bright AGB stars, because their H-rich envelopes quickly become so thin that the stars leave the AGB phase. According to this simple view, an increase of the mass-loss rate induces a corresponding decrease of the foreseen luminosity of the AGB tip. This occurrence has to affect SBF amplitudes. To investigate such an issue quantitatively, we computed a series of SBF models by changing $\eta_{\rm AGB}$ from 0.4 to 3.2. The results in the Johnson-Cousins filters are reported in Table 5 for solar metallicity and the labeled ages. Dealing with AGB stars, the effect is more remarkable in the redder bands. Figure 7 illustrates the SBF dependence on $\eta_{\rm AGB}$ for models with different ages and solar chemical composition in the *IJHK* filters.

Such a dependence provides a unique opportunity to use SBFs to constrain evolutionary parameters during the late stage of the AGB and TP phases. In particular, we calibrate the mass-loss efficiency along the AGB. Each panel of Figure 8 shows the *I*-band SBF predictions computed with a specific value of $\eta_{\rm AGB}$ (0.4, 0.8, 1.6, and 3.2). To perform this calibration we use the mean empirical $\bar{M}_I$ versus $(V-I)_0$ relations derived from observations of galaxies and GGCs. The diagonal solid lines in the range $1.0 \lesssim (V-I)_0 \lesssim 1.3$ represent the relation derived by T01. According to T01 the slope of this relation is quite well established, whereas the

TABLE 5

SBF Amplitudes for Simple Stellar Populations with $Z = 0.02$, $Y = 0.289$, and Different Assumptions for $\eta_{\rm AGB}$

$\eta_{\rm AGB}$	Age	$\bar{M}_U$	$\bar{M}_B$	$\bar{M}_V$	$\bar{M}_R$	$\bar{M}_I$	$\bar{M}_J$	$\bar{M}_H$	$\bar{M}_K$	$V-I$
0.4.....	5	4.122	2.245	0.526	−0.499	−2.047	−5.145	−6.275	−6.803	1.137
	9	4.226	2.350	0.700	−0.279	−1.778	−4.607	−5.731	−6.235	1.192
	11	4.168	2.325	0.711	−0.241	−1.684	−4.448	−5.575	−6.075	1.208
	13	4.111	2.344	0.760	−0.175	−1.598	−4.325	−5.455	−5.950	1.222
	15	4.084	2.353	0.782	−0.153	−1.550	−4.106	−5.236	−5.704	1.237
0.8.....	5	4.124	2.247	0.528	−0.489	−1.918	−4.518	−5.656	−6.145	1.112
	9	4.230	2.352	0.702	−0.270	−1.671	−4.064	−5.190	−5.633	1.174
	11	4.169	2.325	0.710	−0.238	−1.612	−4.025	−5.150	−5.600	1.196
	13	4.111	2.344	0.759	−0.173	−1.526	−3.883	−5.010	−5.447	1.211
	15	4.085	2.353	0.781	−0.152	−1.513	−3.846	−4.974	−5.402	1.229
1.6.....	5	4.127	2.249	0.530	−0.482	−1.849	−4.129	−5.257	−5.697	1.102
	9	4.232	2.353	0.702	−0.268	−1.627	−3.826	−4.949	−5.356	1.166
	11	4.173	2.327	0.712	−0.234	−1.567	−3.745	−4.867	−5.268	1.188
	13	4.116	2.346	0.760	−0.170	−1.485	−3.660	−4.783	−5.184	1.204
	15	4.088	2.354	0.781	−0.150	−1.474	−3.670	−4.795	−5.194	1.222
3.2.....	5	4.130	2.251	0.531	−0.478	−1.794	−3.742	−4.849	−5.204	1.093
	9	4.233	2.352	0.699	−0.269	−1.584	−3.614	−4.731	−5.102	1.158
	11	4.177	2.330	0.714	−0.226	−1.567	−3.583	−4.703	−5.089	1.178
	13	4.121	2.352	0.770	−0.150	−1.415	−3.552	−4.681	−5.082	1.193
	15	4.099	2.377	0.819	−0.093	−1.383	−3.606	−4.741	−5.154	1.208

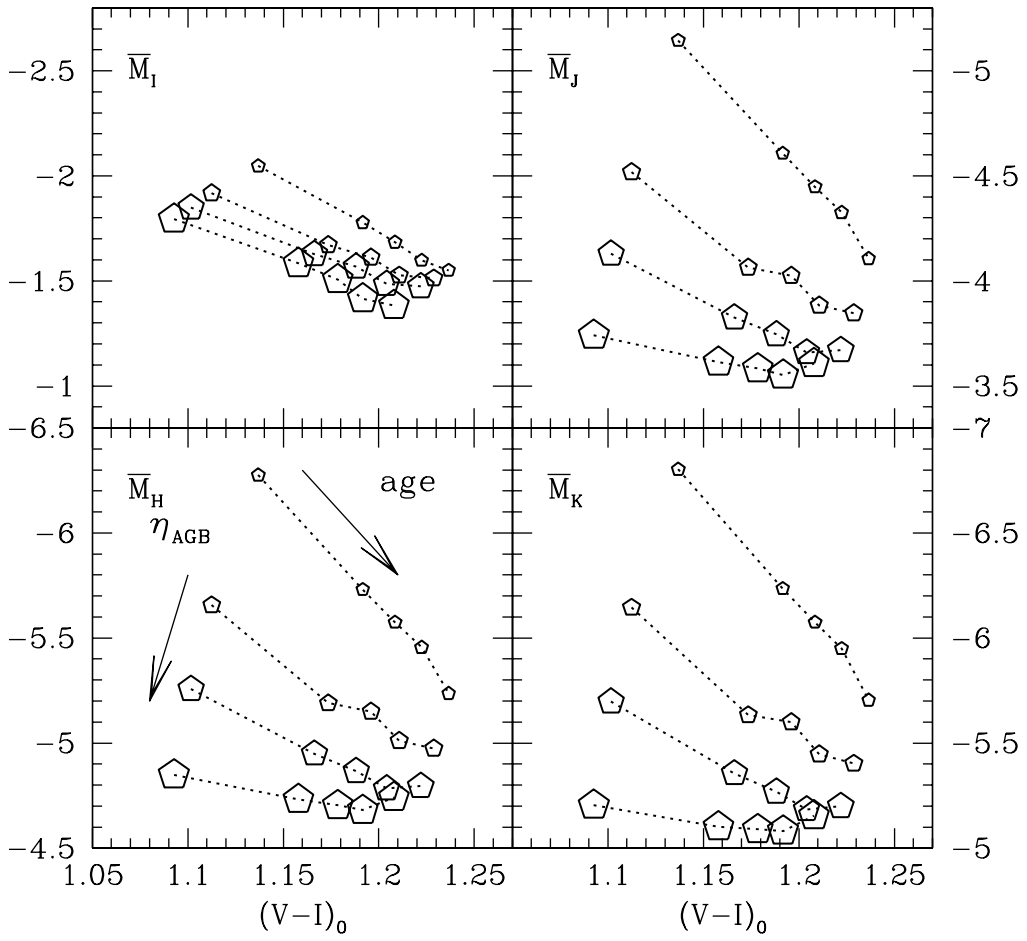

FIG. 7.—Behavior of SBF magnitudes in the *IJHK* bands as functions of $(V-I)_0$ integrated color. A stellar population of solar chemical composition is assumed. The size of the symbols marks increasing values of η_{AGB} (0.4, 0.8, 1.6, and 3.2), as does the orientation of the labeled arrow. The other arrow indicates the orientation of increasing ages (5, 9, 11, 13, and 15 Gyr), which are also linked by dotted lines.

zero point is more uncertain, with an rms scatter as large as 0.1 mag (see Table 4 in TBAD97). However, the true indeterminacy in the zero point is expected to be on the order of 0.20 mag, since one has to include the uncertainties in the Cepheid zero point (Mould et al. 2000; Freedman et al. 2001) and in the LMC distance modulus (e.g., Benedict et al. 2002). The horizontal solid lines in the range $0.8 \lesssim (V-I)_0 \lesssim 1.0$ refer to the observed locus of GGCs (Ajhar & Tonry 1994, hereafter AT94), after a recalibration according to BVA01's prescriptions (eq. [5] in BVA01). In this case the quoted rms scatter is $\sim$0.25 mag. In addition, the zero point of the horizontal line has an indetermination of at least 0.1–0.15 mag, arising from the uncertainty in the GGCs' distances.

Figure 8 shows that the two extreme values of the η_{AGB} do not match the observed SBFs. In fact, $\eta_{AGB} = 0.4$ provides SBF amplitudes that are too bright at all metallicities except $Z = 2\,Z_\odot$; on the contrary, the models with $\eta_{AGB} = 3.2$ appear definitely fainter than observations. The intermediate cases are more interesting: both η_{AGB} values fairly reproduce the SBF data. However, the horizontal line representing the GGC measurements is fitted by SBF simulations of the proper metallicity values but of quite different ages. The assumption of $\eta_{AGB} = 0.8$ leads to a remarkable fit with models of 13–15 Gyr, while $\eta_{AGB} = 1.6$ requires an age on the order of $\sim$9 Gyr. Since our SSP models reproduce the CMDs and integrated properties of GGCs when an age of $\sim$15 Gyr is assumed (BCPR00), we find that $\eta_{AGB} = 0.8$ simulates the mass-loss process on the AGB in such a way that the resulting distribution of stars on the AGB can be reproduced at the same time as the SBF measurements in galaxies and in GGCs.

Despite the large uncertainties on the zero points, this result represents a relevant constraint for stellar evolution models of AGB stars. Even if the exact values of η_{AGB} depend on the assumed theoretical framework, the method outlined here remains a new and powerful tool to improve our knowledge of the details of the evolution of AGB stars.

4.2.3. *Post-AGB Stars*

The theory predicts a small number of PAGB stars (Renzini 1998; BCPR00), which, however, increases with the total number of stars. Though rare objects, PAGB stars cannot be ignored when dealing with populous systems such as galaxies (Greggio & Renzini 1990; Brocato et al. 1990).

For the complex evolution off the asymptotic branch, we rely on the stellar models of Vassiliadis & Wood (1994, hereafter VW94) and Blöcker & Schömberner (1997, hereafter BS97). Since SBFs are sensitive to the most luminous stars, as a first approximation we simulate only the most luminous PAGB, neglecting post–early-AGB evolved stars, which leave the Hayashi track at lower luminosity before the

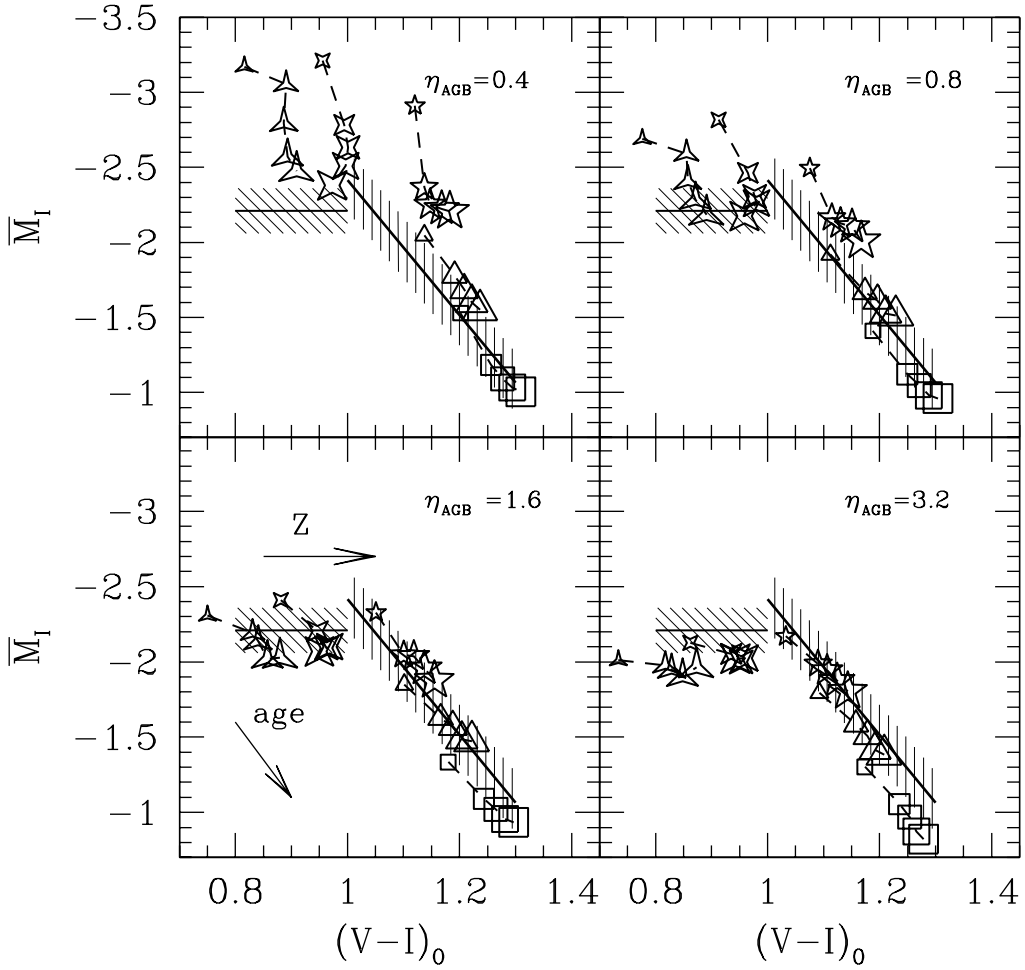

FIG. 8.—Theoretical models obtained by adopting the labeled values of η_{AGB} compared with the empirical calibration of T01 (*diagonal solid lines*). The horizontal solid lines refer to the observational locus of GGCs. Each symbol indicates a different chemical composition: $Z = 0.0001$ (*three-pointed stars*), $Z = 0.001$ (*four-pointed stars*), $Z = 0.01$ (*five-pointed stars*), $Z = 0.02$ (*triangles*), and $Z = 0.04$ (*squares*). The symbol size increases according to age ($t = 5$, 9, 11, 13, and 15 Gyr). The arrows indicate the direction of evolution with age and metallicity. Both the horizontal and the diagonal lines suffer from an uncertainty in the zero point as large as 0.15 and 0.20 mag, respectively (*hatched regions*).

first thermal pulses (Castellani & Tornambé 1991). Under these assumptions, we computed SBF amplitudes for the reference stellar populations with solar metallicity and $t = 15$ Gyr, by simulating a different number of PAGB stars (N_{PAGB}) for the same total number of stars. To perform these simulations, first we evaluated the number of PAGB stars with respect to the number of expected HB stars (N_{HB}) by following the prescriptions of BCPR00. Second, we explored a wide range of values of N_{PAGB}/N_{HB} by artificially varying this ratio.

In Figure 9 we plot the *UBVI*-band SBF amplitudes versus the ratio N_{PAGB}/N_{HB}. The shaded region corresponds to the value of N_{PAGB}/N_{HB} properly derived according to BCPR00. It is apparent that SBFs obtained in filters redder than *V* are not affected by the presence of bright PAGB stars. On the other hand, the *U* and *B* SBFs appear to be quite sensitive to the number of predicted PAGB stars, independent of the assumed stellar evolutionary tracks (VW94; BS97). Here we suggest that precise measurements of *U* and *B* SBFs, with telescopes having high efficiency at such wavelengths (for example, the VLT Survey Telescope),[8] would provide a unique opportunity to derive valuable constraints on the stellar evolution of PAGB stars.

Finally, we find that the luminous and hot stars crossing the CMD from the AGB tip to the beginning of the WD cooling sequence do not appreciably affect the SBF amplitude in most of the bands, except *U* and *B*. We also note that stars evolving down along their WD cooling sequence are not expected to provide a significant contribution in the optical bands. In fact, it becomes more and more negligible as the WD luminosity decreases, even though they pile up because of longer evolutionary times.

4.3. *Impact of Atmosphere Transformations*

The relations transforming the theoretical quantities [$\log L/L_\odot$ and $\log T_{eff}$] into observables (magnitude and colors) are of fundamental importance in modeling SBFs. In general, theoretical relations between colors or bolometric constants and temperatures suffer from the complexity of treating molecular and atomic transitions when the metal content increases and the star temperature decreases. When the metal content grows up to solar or supersolar values, these difficulties become more and more severe because of the formation of grains and complex molecules in the outer

[8] See http://twg.na.astro.it/vst/vst_homepage_twg.html.

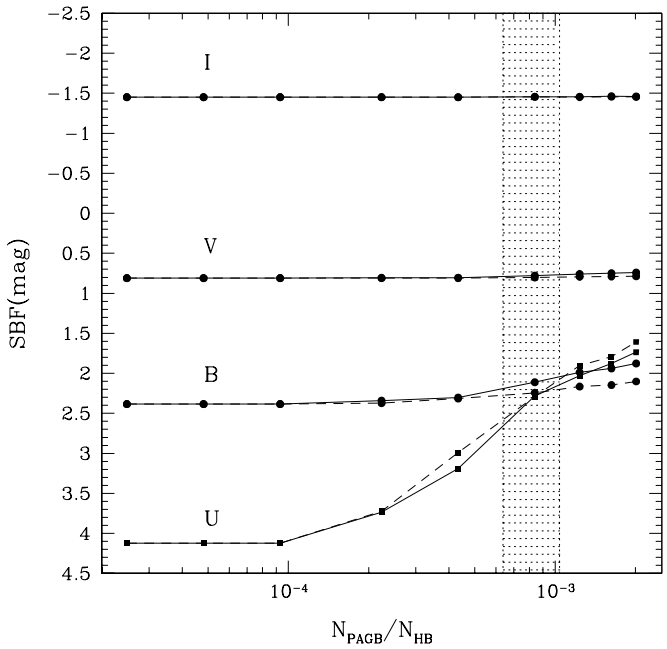

FIG. 9.—Plot of *UBVI*-band SBF magnitudes vs. the number density of PAGB stars relative to HB stars (N_{PAGB}/N_{HB}): BS97 (*solid lines*) and VW94 PAGB (*dashed lines*) models. The shaded region indicates the proper ratio predicted for our reference models. A solar-metallicity population ($Z = 0.02$) with age $t = 15$ Gyr is assumed.

part of the atmosphere, which causes strong blanketing effects (Bell 1973). On the other hand, empirical compilations involve difficulties in deriving fundamental star parameters, such as metallicity and gravity, from observed spectra and colors (Alonso, Arribas, & Martínez-Roger 1996, 1999).

In this section we evaluate how SBF amplitudes change by adopting different transformation tables available in the literature. To provide a quantitative comparison we selected three color-temperature compilations commonly used for synthetic stellar population models: the theoretical tabulation of Castelli, Gratton, & Kurucz (1997, hereafter CGK97), the hybrid library of LCB97, and the semiempirical Yale transformations (Green, Demarque, & King 1987, hereafter GDK87). The CGK97 tabulation is the result of the atmosphere models obtained with the updated Kurucz code. The LCB97 corrected tabulations are based on theoretical spectra from different authors, properly adapted to match observations (see LCB97 for more details). The semiempirical tables proposed by the Yale group result from the calibration of the old Kurucz (1979) models. Both CGK97 and LCB97 include all the ground-based Johnson-Cousins filters (*UBVRIJHK*), while the GDK87 tables cover only the optical range (*UBVRI*).

We computed a set of stellar population models for the selected metallicities, $t = 15$ Gyr, and with the reference assumptions for mass loss and IMF. For each model, we evaluated SBF amplitudes by adopting all three tabulations mentioned above.

The results are reported in Table 6. The relative differences in the SBF amplitudes for selected filters (*UBVRIJHK*) are plotted in Figure 10 as a function of the population metal content Z for a fixed age. The differences are computed relative to the LCB97 model. For $Z < 0.01$, Figure 10 shows that SBF amplitudes are quite well determined. In this metallicity range (GGCs) there are differences $\lesssim 0.2$ mag using either the model of CGK97 or LCB97 or GDK87, a fact supporting the reliability of SBF models of these metallicities.

The situation worsens for higher metallicities. For $Z > 0.01$, the GDK87 transformations lead to systematically brighter SBF amplitudes in all the considered bands (up to more than 1 mag for the I band). Such a large difference may be due to the fact that the GDK87

TABLE 6
SBF AMPLITUDES FOR DIFFERENT COLOR-TEMPERATURE RELATIONS

Z	$\bar{M}_U$	$\bar{M}_B$	$\bar{M}_V$	$\bar{M}_R$	$\bar{M}_I$	$\bar{M}_J$	$\bar{M}_H$	$\bar{M}_K$
LCB97 Atmosphere Transformations								
0.0001	1.533	0.811	−0.610	−1.424	−2.184	−3.101	−3.751	−3.923
0.001	2.008	1.080	−0.424	−1.330	−2.173	−3.215	−4.056	−4.244
0.01	3.324	1.926	0.331	−1.697	−2.011	−3.644	−4.732	−5.081
0.02	4.085	2.352	0.781	−1.152	−1.512	−3.846	−4.973	−5.402
0.04	4.740	2.786	1.198	0.305	−0.960	−3.881	−5.012	−5.521
CGK97 Atmosphere Transformations								
0.0001	1.579	0.817	−0.522	−1.271	−2.004	−3.142	−3.869	−4.048
0.001	2.108	1.072	−0.427	−1.259	−2.050	−3.281	−4.161	−4.368
0.01	3.433	1.863	0.128	−0.850	−1.933	−3.661	−4.830	−5.145
0.02	4.094	2.253	0.496	−0.510	−1.474	−3.815	−5.094	−5.416
0.04	4.844	2.660	0.878	−0.125	−1.121	−3.803	−5.218	−5.585
GDK87 Atmospheres Transformations								
0.0001	1.587	0.828	−0.432	−1.248	−1.943	...	...	...
0.001	2.067	1.037	−0.426	−1.274	−2.044	...	...	...
0.01	3.013	1.769	0.151	−0.850	−2.087	...	...	...
0.02	3.355	2.049	0.515	−0.468	−2.033	...	...	...
0.04	3.743	2.338	0.863	-0.075	-2.084	...	...	...

NOTE.—An age $t = 15$ Gyr is assumed.

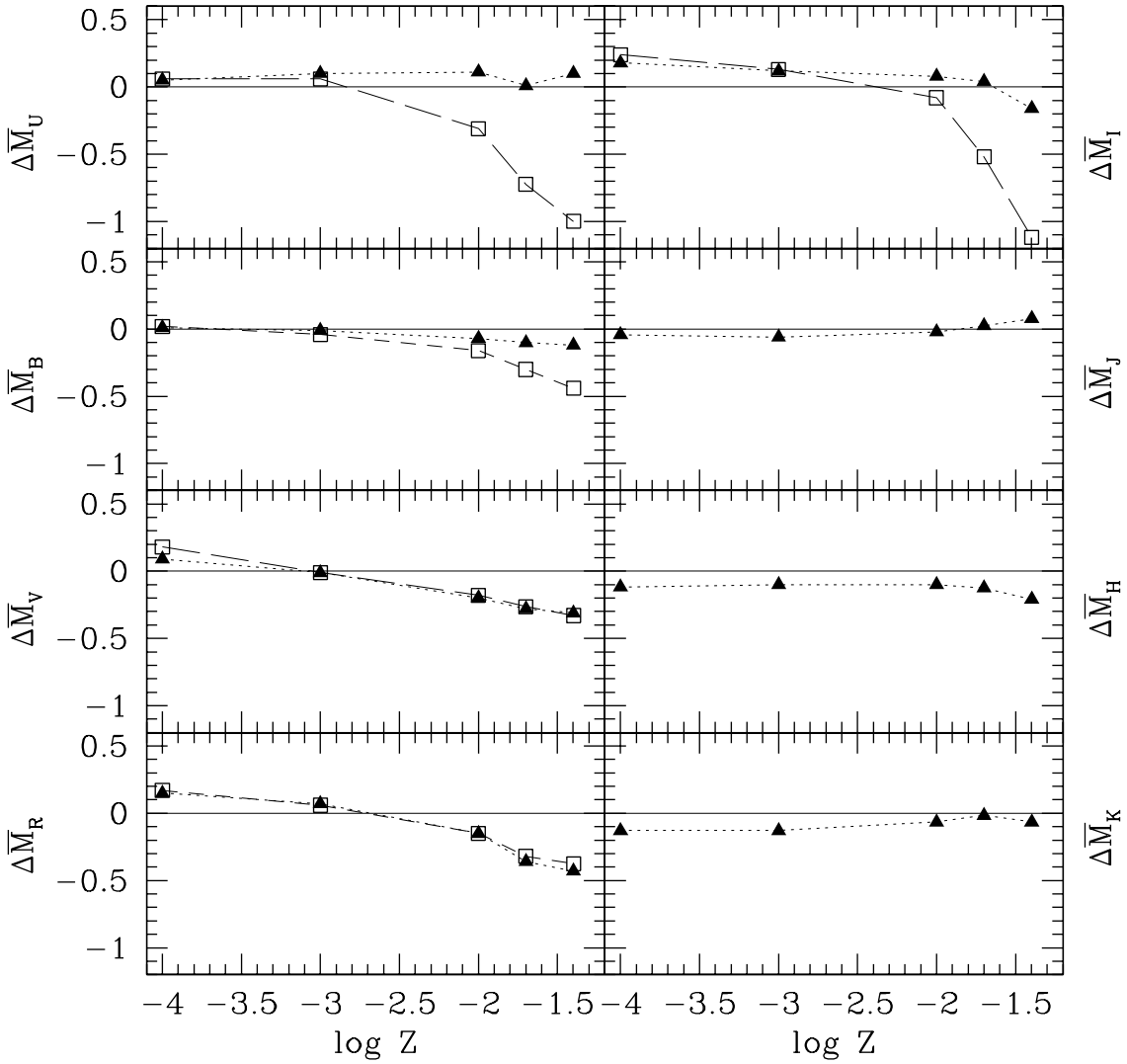

FIG. 10.—Effects of transformation tables on SBF amplitudes, illustrated as a function of metallicity. The residuals are computed as $\Delta\bar{M} = \mathrm{SBF}_X - \mathrm{SBF}_{\mathrm{LCB97}}$, where X = CGK97 (*dotted lines*, *filled triangles*) or X = GDK87 (*long-dashed lines*, *open squares*). An age of $t = 15$ Gyr is considered.

transformations have been calibrated with GGCs, which are low-metallicity objects. The LCB97 and CGK97 models give quite similar predictions for all the optical and NIR bands. Sizable differences are only expected in the V and R bands, where the SBFs are about 0.3 mag brighter in the CGK97 models.

In order to understand the origin of these differences, we show the color-magnitude location of the most luminous stars of a solar-metallicity isochrone aged 15 Gyr transformed by adopting all the quoted compilations. For clarity, we focus our attention on the RGB stars, bearing in mind that AGB stars behave similarly. We consider as representative the $[M_V, (V-I)_0]$, $[M_I, (V-I)_0]$, and $[M_K, (V-I)_0]$ diagrams in Figure 11. The isochrones mapped in the observational plane by using the GDK87 transformations provide a much brighter RGB tip (where stars reach temperatures lower than 3500 K) in the I band (Fig. 11, *middle*) compared with those of LCB97 (and CGK97); this could explain the brighter I-band SBF amplitude obtained by using the GDK87 model. Moreover, since the RGB-tip magnitude calculated with the LCB97 model is fainter than those calculated with CGK97's for all bands, one expects SBFs to become fainter and colors redder for metallicity higher than solar when the LCB97 model is adopted, exactly as shown by Figure 10.

In Figure 11 we also plot the isochrones transformed using the empirical color-temperature relations published by Alonso et al. (1996, 1999), since they are used in the BVA01 SBF models. We note that the *RI* filters involved in the Alonso et al. transformations are the Johnson & Morgan (1953) bands, as opposed to the Cousins (1976, 1978) passbands commonly used for SBF observations. By applying the relations to convert $V-I_J$ into $V-I_C$ (in Fig. 11 we used Bessel 1979), the differences become negligible, making the Alonso et al. models similar to the others in their own temperature range. A significant disadvantage of this grid is that it is limited to $T_{\mathrm{eff}} \geq 3750$ K for $[\mathrm{Fe/H}] > -1.0$, and therefore one needs to extrapolate or to merge with other tables down to lower temperatures. For all these reasons we decided not to use these color-temperature relations in computing SBFs.

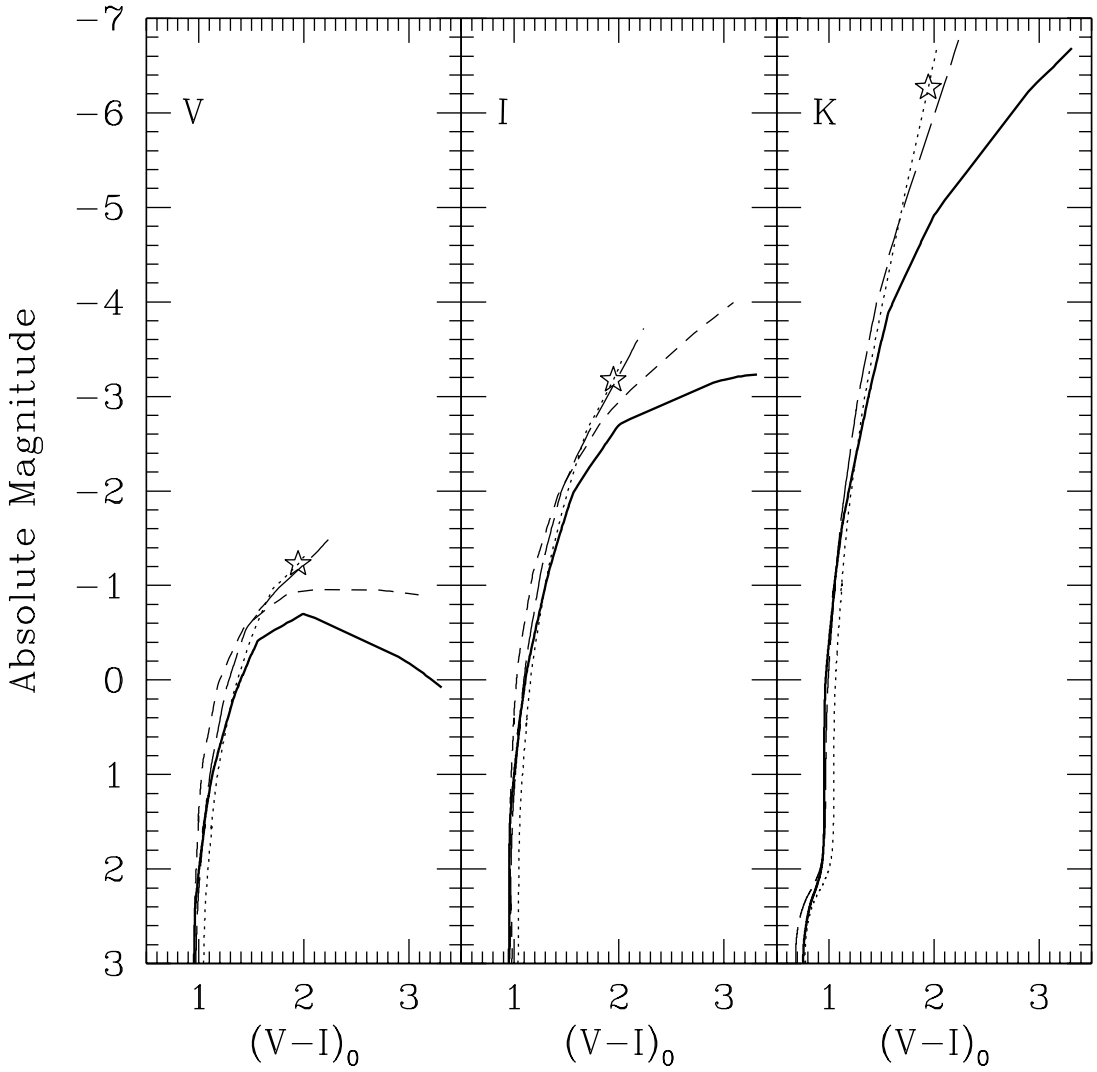

FIG. 11.—The solar-metallicity isochrone ($t = 15$ Gyr) is transformed according to LCB97 (*heavy solid line*), CGK97 (*dotted line*), GDK87 (*dashed line*), and Alonso et al. (1996, 1999; *long-dashed line*). *From left to right*: V vs. $(V-I)_0$, I vs. $(V-I)_0$, and K vs. $(V-I)_0$. The five-pointed star indicates where the extrapolation from colors for CGK97 tables ($T_{\rm eff} < 3500$ K) begins. Alonso et al. (1999) models have nearly the same limit, the minimum temperature being tabulated as $T_{\rm min} = 3750$ K.

5. COMPARISON WITH THE OBSERVATIONAL DATA

As a first step we compare our SBF predictions in several bands with actual observations of stellar systems (GGCs and galaxies) with known distances. Then the theoretical SBFs are used to derive the characteristics of a selected sample of observed stellar populations.

5.1. *Galactic Globular Clusters*

The only SBF measurements related to GGCs are those by AT94 for a sample of 19 objects. There are several reasons to study the SBFs of these objects: (1) GGCs span a range of metallicity down to values lower than expected in galaxies; (2) since they are thought to be formed by the gravitational collapse of a homogeneous gas cloud, they are the best observational counterpart of theoretical SSPs; and (3) the SBFs of GGCs are determined directly from their resolved stars (differently than galaxies, which require a more complex analysis). Thus, GGC SBFs represent a simple and unambiguous target with which to verify the stellar evolution assumptions.

Before going on, it is worth noting that since the number of stars in a globular cluster (10^5–10^6) is far lower than the stellar content in a typical galaxy ($>10^{10}$), this might bear on the SBF evaluations for statistical reasons. Consequently, the proper way to evaluate theoretical SBFs for GGCs is to compute simulated CMDs (with total number of stars $N_{\rm star} \sim 10^6$) and directly apply equations (7)–(9) of TS88. Despite the difference in the total number of stars, the resulting SBFs are quite similar (within the uncertainties) to the values for $Z \leq 0.006$ derived from the procedure presented in § 1 (Table 1). Such stability in the computed SBF amplitudes is due to the compensation of two conflicting effects that arise when the size of the simulated stellar population decreases. On the one hand, the number of stars expected in the fastest and brightest evolutionary phases (e.g., TP, AGB) tends to vanish, and fainter SBF amplitudes are obtained. On the other hand, the number of bright RGB stars decreases, providing a less populated RGB; statistical

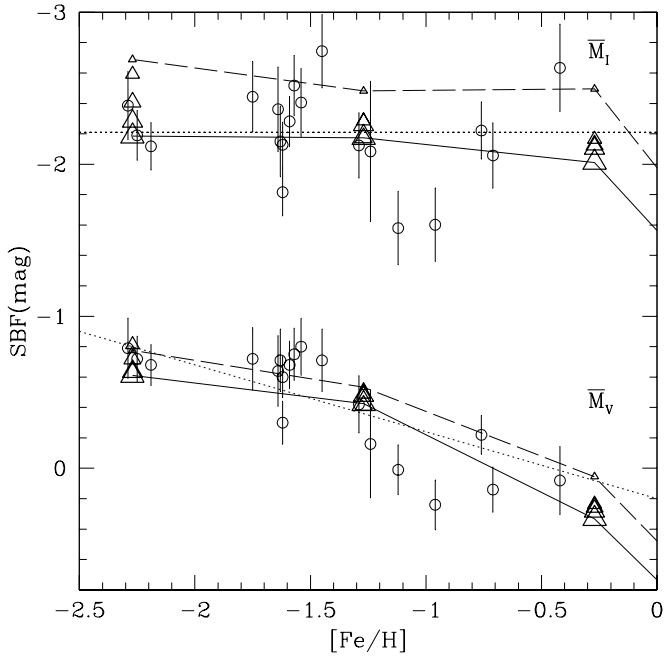

FIG. 12.—Our SBF predictions (*open triangles*) in V and I bands plotted against the observational data of 19 GGCs (AT94; *open circles*). Models of increasing age are marked with larger symbols ($t = 5$, 9, 11, 13, and 15 Gyr); the solid line and the long-dashed line connect models with $t = 15$ and 5 Gyr, respectively, for different chemical compositions. Dotted lines represent the best-fit as derived by BVA01 (see text).

effects become relevant (see also BCPR00), leading to brighter SBF amplitudes.

Since AT94 measurements are only available for VI bands, the comparison with theoretical models can be done only for these two filters. In Figure 12 the GGC observational data are compared with our models. The observational absolute SBF magnitudes for each globular cluster are obtained from the AT94 data according to the expression $\bar{M}_X = \bar{m}_X - \mathrm{DM}$, where DM is the distance modulus. The latter quantity, the metallicity, and other properties are from the latest version of the electronic catalog compiled by Harris (1996)[9]; and are summarized in Table 7, which also reports the observed SBF values. In the figure the solid and dashed lines connect the oldest and youngest models, respectively, with different metallicities. The dotted lines represent the mean line according to BVA01's prescriptions (their eq. [5]). From Figure 12 it is apparent that (1) DMs derived directly from theoretical SBFs are in very good agreement with the recent evaluations from other distance indicators, and (2) the general trend of observed SBFs versus metallicity is well reproduced by theoretical models. This fact is noteworthy because the [Fe/H] values of GGCs are measured directly and not just derived via integrated colors. Finally, let us note that the good agreement between the single measurements and the models is particularly relevant considering that no effort has been put into reproducing the peculiarities of each individual GGC (HB morphology, brightest stars, etc.).

5.2. *The Galaxy Sample*

Unfortunately, no GGC with $Z \gtrsim 1\ Z_\odot$ is known, and one needs to look at elliptical galaxies and bulges of spirals to verify the degree of accuracy of SBF predictions for metal-rich populations. For this purpose, we extract a subsample of galaxies from the T01 I-band database by selecting objects with reliable distance estimates as derived by Ferrarese et al. (2000). The result is given in Table 8, in which the data for 31 galaxies are summarized. In the table we report from, left to right, the galaxy name, morphological type T, absorption A_B, integrated color $(V-I)_0$, and the SBF apparent magnitudes in I, V, R, K', K_s, F814W, and F160W filters. The last column reports the galaxy distance derived from Cepheids, when available (eight galaxies); otherwise the average distance from other indicators (Ferrarese et al. 2000) is listed. We note that for the sample of galaxies with Cepheid-based distances, the new calibrations of the

[9] See http://physun.physics.mcmaster.ca/Globular.html (1999 version).

TABLE 7
MEASURED SBF AMPLITUDES

Cluster	$\bar{m}_V$	$\bar{m}_I$	E_{B-V}	$(V-I)_0$	M_V^{tot}	[Fe/H]	DM
NGC 104 (47 Tuc)	13.15 ± 0.08	11.10 ± 0.16	0.04	1.06	−9.42	−0.76	13.37
NGC 288	14.53 ± 0.34	12.57 ± 0.45	0.03	0.92	−6.60	−1.24	14.69
NGC 2419	19.29 ± 0.09	17.72 ± 0.12	0.11	0.85	−9.58	−2.34	19.97
NGC 5139	13.67 ± 0.10	12.01 ± 0.12	0.12	0.95	−10.29	−1.62	13.97
NGC 5272 (M3)	14.37 ± 0.14	12.59 ± 0.17	0.01	0.88	−8.93	−1.57	15.12
NGC 5904 (M5)	14.04 ± 0.16	12.30 ± 0.19	0.03	0.89	−8.81	−1.29	14.46
NGC 6093 (M80)	14.84 ± 0.18	12.90 ± 0.21	0.18	0.99	−8.23	−1.75	15.56
NGC 6205 (M13)	13.68 ± 0.16	12.05 ± 0.20	0.02	0.88	−8.70	−1.54	14.48
NGC 6341 (M92)	13.85 ± 0.17	12.23 ± 0.20	0.02	0.86	−8.20	−2.29	14.64
NGC 6624	15.45 ± 0.20	12.40 ± 0.27	0.28	1.20	−7.50	−0.42	15.37
NGC 6626 (M28)	14.41 ± 0.18	11.86 ± 0.22	0.43	1.01	−8.33	−1.45	15.12
NGC 6637 (M69)	15.30 ± 0.11	12.91 ± 0.19	0.16	1.07	−7.52	−0.71	15.16
NGC 6652	15.43 ± 0.13	13.48 ± 0.22	0.09	1.03	−7.73	−0.96	15.19
NGC 6656 (M22)	12.96 ± 0.21	10.83 ± 0.26	0.34	1.00	−8.50	−1.64	13.60
NGC 6715 (M54)	16.93 ± 0.12	15.16 ± 0.13	0.14	0.90	−10.01	−1.59	17.61
NGC 6723	14.88 ± 0.13	13.23 ± 0.22	0.05	1.01	−7.86	−1.12	14.87
NGC 7006	17.53 ± 0.18	16.03 ± 0.21	0.05	0.92	−7.68	−1.63	18.24
NGC 7078 (M15)	14.65 ± 0.11	13.06 ± 0.13	0.10	0.83	−9.17	−2.25	15.37
NGC 7089 (M2)	14.89 ± 0.09	13.29 ± 0.11	0.06	0.91	−9.02	−1.62	15.49

NOTES.—The values for $\bar{m}_V$ and $\bar{m}_I$, and $(V-I)_0$ color are from AT94. Other GGC properties are from Harris 1996.

TABLE 8

SELECTED GALAXY SAMPLE

Galaxy	T[a]	A_B[a]	$(V-I)_0$[a]	$\bar{m}_I$[a]	$\bar{m}_V$	Ref.	$\bar{m}_R$	Ref.	$\bar{m}_{K'}$	Ref.	$\bar{m}_{Ks}$	Ref.	$\bar{m}_{F814W}$	Ref.	$\bar{m}_{F160W}$	Ref.	DM
Cepheid Distance Determination																	
N0224	3	0.35	1.231 ± 0.007	23.03 ± 0.05	25.29 ± 0.08	1	...		18.80 ± 0.21	5	18.82 ± 0.09	8	23.54 ± 0.04	11	19.78 ± 0.04	14	24.44 ± 0.10
N3031	2	0.35	1.187 ± 0.011	26.38 ± 0.25	29.07 ± 0.27	1	...		...		...		...		22.99 ± 0.05	14	27.80 ± 0.08
N3351		0.12	1.225 ± 0.014	...	...		...		...		...		...		25.19 ± 0.07	14	30.01 ± 0.08
N3368	2	0.11	1.145 ± 0.015	28.32 ± 0.20	...		...		...		...		...		24.88 ± 0.09	14	30.20 ± 0.10
N4258	4	0.07	1.134 ± 0.023	27.50 ± 0.08	...		...		...		...		...		...		29.49 ± 0.07[b]
N4548	3	0.16	1.148 ± 0.019	29.67 ± 0.53	...		...		...		...		...		...		31.04 ± 0.08
N4725	2	0.05	1.209 ± 0.023	29.14 ± 0.32	...		...		...		...		...		25.72 ± 0.10	14	30.57 ± 0.08
N7331	3	0.39	1.120 ± 0.017	28.72 ± 0.14	...		...		...		...		...		25.43 ± 0.08	14	30.89 ± 0.10
Other Distance Determination																	
N0221	−6	0.35	1.133 ± 0.007	22.73 ± 0.05	25.14 ± 0.10	2	24.36 ± 0.10	2	18.56 ± 0.09	6	18.56 ± 0.08	8	22.84 ± 0.03	11	19.11 ± 0.05	14	24.56 ± 0.17
N0891	3	0.28	1.142 ± 0.017	27.83 ± 0.11	...		...		...		...		...		...		29.95 ± 0.05
N1023	−3	0.26	1.193 ± 0.017	28.74 ± 0.13	...		...		...		...		29.11 ± 0.04	11	...		30.23 ± 0.08
N1316	−2	0.09	1.132 ± 0.016	29.83 ± 0.15	32.25 ± 0.16	3	...		...		...		...		26.11 ± 0.09	14	31.28 ± 0.09
N1399	−5	0.06	1.227 ± 0.016	30.11 ± 0.13	32.47 ± 0.12	3	...		25.98 ± 0.16	7	26.14 ± 0.12	9	...		26.79 ± 0.04	14	31.31 ± 0.09
N1404	−5	0.05	1.224 ± 0.016	30.20 ± 0.16	32.48 ± 0.12	3	...		25.82 ± 0.14	7	25.89 ± 0.05	9	...		26.69 ± 0.08	14	31.33 ± 0.10
N3115	−3	0.20	1.183 ± 0.010	28.34 ± 0.06	...		...		...		...		...		...		30.05 ± 0.10
N3377	−5	0.15	1.114 ± 0.009	28.35 ± 0.06	30.57 ± 0.11	1	...		...		...		28.59 ± 0.05	11	...		30.19 ± 0.08
N3379	−5	0.10	1.193 ± 0.015	28.57 ± 0.07	31.21 ± 0.06	2	30.36 ± 0.05	2	...		24.72 ± 0.06	10	28.81 ± 0.11	12	25.26 ± 0.08	14	30.23 ± 0.06
N3384	−3	0.11	1.151 ± 0.018	28.59 ± 0.10	...		...		...		...		28.87 ± 0.02	11	25.34 ± 0.17	14	30.28 ± 0.08
N4278	−5	0.12	1.161 ± 0.012	29.34 ± 0.18	...		...		...		...		...		26.38 ± 0.09	14	30.51 ± 0.14
N4374	−5	0.17	1.191 ± 0.008	29.77 ± 0.09	32.02 ± 0.09	2	31.22 ± 0.07	2	...		25.43 ± 0.22	8	30.02 ± 0.01	13	...		31.20 ± 0.10
N4382	−1	0.13	1.150 ± 0.022	29.59 ± 0.09	...		...		...		...		...		...		31.07 ± 0.11
N4406	−5	0.13	1.167 ± 0.008	29.51 ± 0.12	32.11 ± 0.10	2	31.23 ± 0.06	2	25.45 ± 0.10	7	...		30.10 ± 0.03	13	26.26 ± 0.06	14	31.22 ± 0.07
N4472	−5	0.10	1.218 ± 0.011	29.62 ± 0.07	32.26 ± 0.06	2	31.27 ± 0.06	2	25.30 ± 0.11	7	25.25 ± 0.13	8	29.99 ± 0.02	13	26.26 ± 0.04	14	31.07 ± 0.08
N4486	−4	0.10	1.244 ± 0.012	29.72 ± 0.14	...		...		...		...		30.07 ± 0.03	13	...		30.97 ± 0.10
N4494	−5	0.09	1.139 ± 0.010	29.38 ± 0.08	...		...		...		...		...		...		30.81 ± 0.08
N4565	3	0.07	1.128 ± 0.027	29.37 ± 0.11	...		...		...		...		...		25.53 ± 0.08	14	30.63 ± 0.12
N4649	−5	0.12	1.232 ± 0.023	29.76 ± 0.09	...		...		...		...		30.21 ± 0.07	13	...		31.09 ± 0.08
N4660	−5	0.14	1.154 ± 0.015	28.82 ± 0.17	...		...		...		...		30.11 ± 0.09	13	...		30.70 ± 0.08
N5102	−3	0.24	0.976 ± 0.016	25.49 ± 0.09	...		...		...		...		...		...		27.89 ± 0.13
N5128	−2	0.50	1.078 ± 0.016	26.05 ± 0.11	28.12 ± 0.06	4	...		...		...		...		...		27.90 ± 0.08
N5195	0	0.16	1.056 ± 0.019	27.25 ± 0.25	...		...		...		...		...		...		29.37 ± 0.08

[a] Data from T01.

[b] Freedman et al. 2001, Table 3.

REFERENCES.—(1) Ajhar & Tonry 1994; (2) Tonry et al. 1990; (3) Blakeslee et al. 2001; (4) Tonry & Schetcher 1990; (5) Jensen et al. 1996; (6) Luppino & Tonry 1993; (7) Jensen et al. 1998; (8) Pahre & Mould 1994; (9) LGC02; (10) Mei et al. 2001; (11) Ajhar et al. 1997; (12) Pahre et al. 1999; (13) Neilsen & Tsvetanov 2000; (14) Jensen et al. 2003.

period-luminosity (PL) and period-luminosity-metallicity (PLZ) relations by Freedman et al. (2001) lead to DMs that differ on average by $\Delta DM_{PL} = 0.13 \pm 0.06$ and $\Delta DM_{PLZ} = 0.03 \pm 0.05$, respectively. Since the debate on the PL and PLZ relations is still open, we adopt the Ferrarese et al. database for the sake of homogeneity and clarity.

We test the consistency of our predicted SBFs starting from galaxies with distance evaluations based on Cepheids, as they are the most reliable distance indicator. Since the SBF method works at its best with spheroidal galaxies, there is a relative scarcity of SBF measurements for spirals, and even fewer objects with both SBF and Cepheid distance determinations. We first focus our attention on the *I* band, because of its importance in the calibration of the empirical relation (T01), and then we extend the analysis to other photometric bands. Figure 13 illustrates the comparison of the sampled galaxies with the present models; the empirical line of T01 is also plotted. The figure shows that all the galaxies match the theoretical models well, with $(V-I)_0 > 1.0$ mag. We emphasize that the zero point of the empirical relation of T01 is derived directly from Cepheid-calibrated distances, while the present theoretical SBFs are completely independent of them. At $(V-I)_0 < 1.0$ the theory predicts a nearly constant value of *I*-band SBFs for models of similar age, as already verified by GGC measurements. Moreover, this appears to be in agreement with the location of the galaxy NGC 5253 (not plotted in the figure) reported in Figure 8 of BVA01.

If we extend the comparison to all the galaxies in Table 8 (Fig. 14), the agreement remains good, even though a few of the observed values appear fainter than those predicted by the theory and by the empirical line. We note that the galaxies showing the largest scatter (NGC 4278 and NGC 4565) have distance measurements with quite a large spread, if compared with internal uncertainties (Ferrarese et al. 2000).

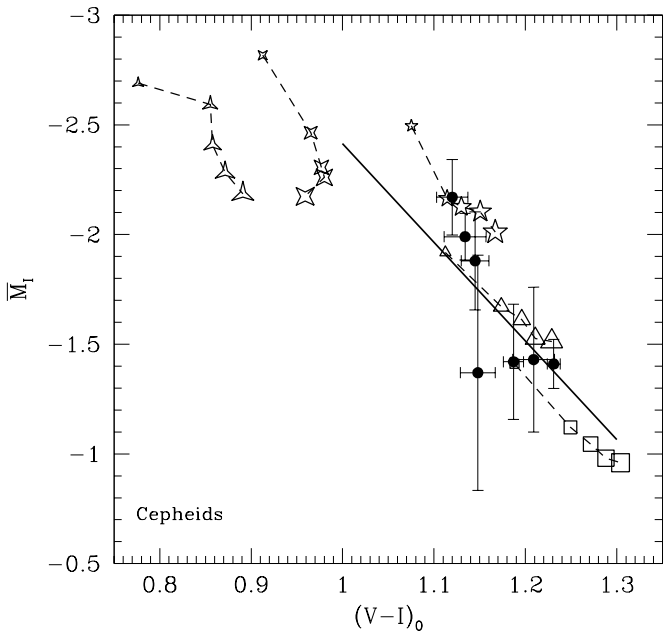

FIG. 13.—Theoretical *I*-band SBFs compared with observed data; $\bar{M}_I$ for observed galaxies was derived by adopting the DMs from the period-luminosity relation of Cepheid variables (Ferrarese et al. 2000). Symbols are as in Fig. 8.

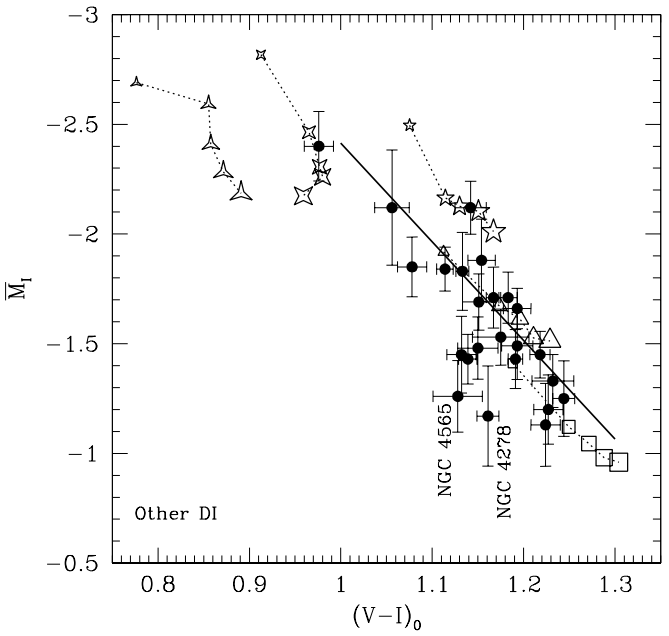

FIG. 14.—Same as Fig. 13, but for a sample of galaxies with distances measured by other distance indicators. DMs are again from Ferrarese et al. (2000).

Taking advantage of multiband observations, in Figure 15 we report a similar comparison for *V*, *K*, and F160W filters. Following Jensen et al. (2001), we discard NGC 4536 from their sample because its anomalous F160W-band SBF magnitude appears to be due to clumpy dust contamination. Figure 15 shows that our theoretical predictions are consistent with observations not only in the *I* band, but also in other selected optical and NIR filters. This result is relevant for two reasons. First, the agreement of the absolute values of the SBF amplitudes suggests that the present theoretical SBF, computed in the other selected photometric bands, may also be adopted to derive distances. Second, the agreement over a wide range of wavelengths supports the reliability of the global theoretical assumptions for the stellar population from which we derive the SBFs.

Since the proposed theoretical framework is supported by SBF observations, at least in the main relevant features, we are led to push forward the capability of the SBF technique and to tentatively infer information on age and metallicity from the SBF measurements of the quoted sample of galaxies.

5.3. *SBFs as Stellar Population Tracers*

Once the distance of an object is known, or in the case of several objects all at the same distance (e.g., cluster galaxies), one may want to use the SBF models for deriving ages and metallicities of the stellar populations. To this end we test the internal consistency of the SBF models in various bands, basically *V*, *I*, *K*, and F160W. Further, we verify the reliability of the inferred (average) age and metallicity through comparison with literature values derived by other methods.

The problem of evaluating the age and metallicity of stellar populations in elliptical galaxies is a highly debated topic (see, for example, Henry & Worthey 1999 and references therein). Thus, to select measurements or evaluations of

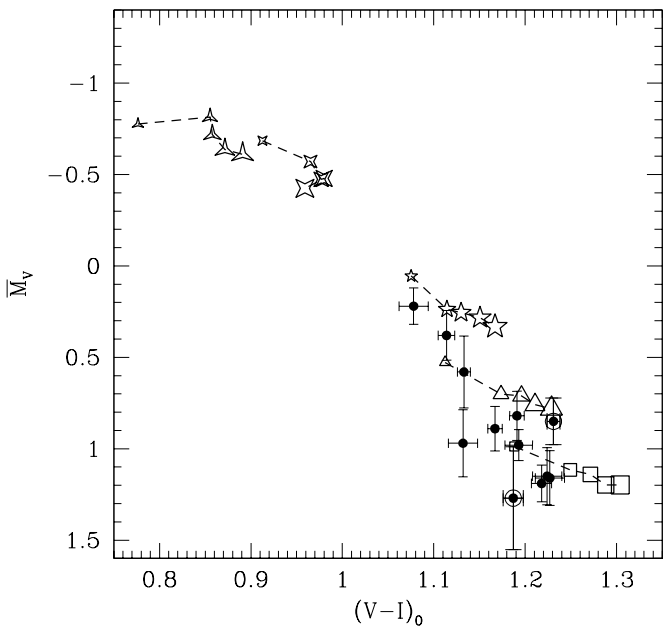

FIG. 15*a*

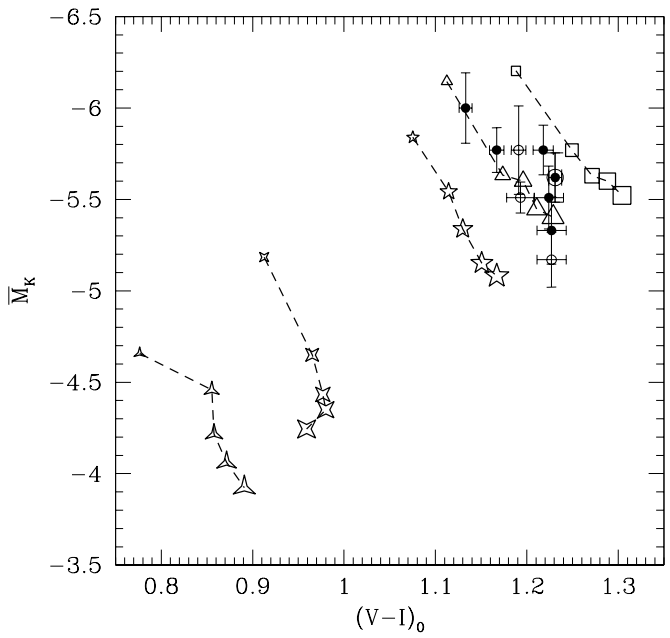

FIG. 15*b*

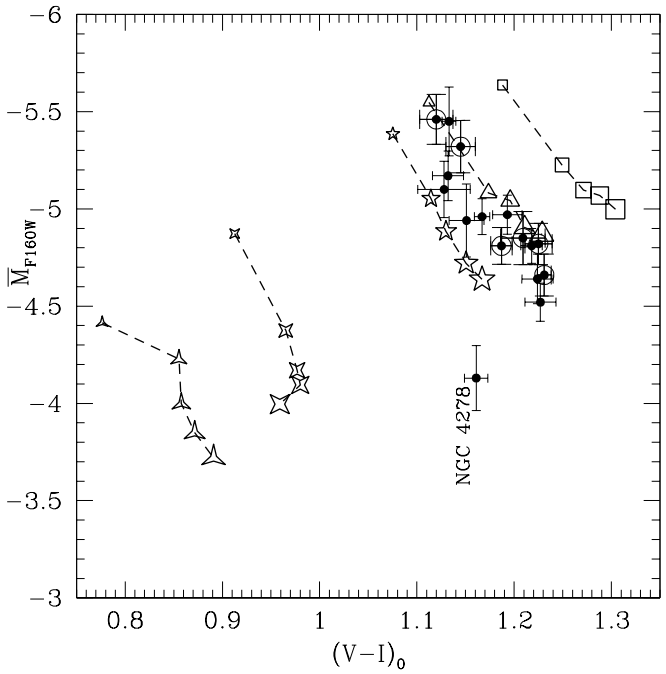

FIG. 15*c*

FIG. 15.—(*a*) Same as Fig. 14, but for $\bar{M}_V$. Galaxies with Cepheid-based distances are added (*circled points*). (*b*) Same as (*a*), but for $\bar{M}_K$. Filled circles are K' measurements, while open circles are K_s. Galaxies with multiple observations are still plotted using different symbols. (*c*) Same as (*a*), but for $\bar{M}_{F160W}$. We note that NGC 4278 has distance measurements with a large spread compared with internal uncertainties (Ferrarese et al. 2000).

those quantities that can probe the reliability of SBF models in deriving t and Z is a quite a difficult step. For example, one is faced with the problem that elliptical galaxies are made up of complex stellar populations, i.e., of mixed age and metallicity populations (e.g., Baugh, Cole, & Frenk 1996; Kauffmann & Charlot 1998; Saglia et al. 2002), while we use the approximation of a single-burst stellar population. Another difficulty comes from the evidence that gradients in metallicity, age, or both are observed in some elliptical galaxies (Peletier et al. 1990; Carollo, Danziger, & Buson 1993; Kobayashi & Arimoto 1999). As a further complication, SBF measurements and (t, Z) evaluations from other indicators may refer to non-overlapping regions of the studied galaxy.

Keeping in mind the quoted (relevant) warnings, it is still interesting to evaluate ages and metallicities from SBF measurements by using the present theoretical models. Clearly, the following results refer to SBFs measured in relatively extended galaxy regions, and they are valid in the approximation that in these regions there is a dominant

TABLE 9
AGE AND METALLICITY ESTIMATIONS FOR SELECTED GALAXIES

Galaxy (1)	DM (2)	Age[a] (3)	[Fe/H][a] (4)	Age[b] (5)	[Fe/H][b] (6)	Age^{SBF}_{mag} (7)	$[Fe/H]^{SBF}_{mag}$ (8)	Age^{SBF}_{color} (9)	$[Fe/H]^{SBF}_{color}$ (10)
NGC 221	24.44 ± 0.10	3.8	−0.04	4.9 ± 1.3	-0.01 ± 0.05	5–9	∼0.00	6	0.04
NGC 224	24.44 ± 0.07	5.1	0.42	...	...	∼15	∼0.00	12	0.15
NGC 891	29.96 ± 0.06	11	−0.47	...	...	11–13	∼−0.27	...	...
NGC 1316.....	31.49 ± 0.03	3.4	0.25	...	...	∼5	∼0.00	...	...
NGC 1399.....	31.49 ± 0.03	...	>0.5	...	...	$\gtrsim$10	$\gtrsim$0.00	12	0.12
NGC 1404.....	31.49 ± 0.03	5.9	0.47	...	...	5–9	$\gtrsim$0.00	9	0.20
NGC 3115.....	30.14 ± 0.16	...	>0.5	...	...	∼13	0.00/−0.27	...	...
NGC 3377.....	30.09 ± 0.04	4.1	0.20	5.9 ± 1.2	-0.28 ± 0.04	∼5	0.00	...	...
NGC 3379.....	30.09 ± 0.04	9.3	0.16	13.2 ± 2.4	-0.17 ± 0.04	9–13	∼0.00	12	0.00
NGC 3384.....	30.09 ± 0.04	...	>0.5	...	...	∼5	0.00/0.33[c]	...	...
						13	−0.27[d]		
NGC 4278.....	31.11 ± 0.09	10.7	0.14	...	...	5–9	0.00[c]	...	...
						13–15	−0.27[d]		
NGC 4374.....	30.97 ± 0.04	11.8	0.12	14.4 ± 2.8	-0.19 ± 0.05	5–11	$\gtrsim$0.00	8	0.15
NGC 4382.....	30.97 ± 0.04	1.6	0.44	...	...	$\lesssim$5	$\gtrsim$0.33	...	...
NGC 4472.....	31.01 ± 0.04	8.5	0.24	8.4 ± 2.7	0.00 ± 0.06	$\gtrsim$7	$\gtrsim$0.00	9	0.20
NGC 4649.....	31.54 ± 0.08	11	0.30	18.3 ± 2.8	-0.22 ± 0.04	...	...	...	...

[a] Terlevich & Forbes 2002, Table 2.
[b] Trager et al. 2000, Table 6B: model 4.
[c] Estimations from $\bar{M}_I$.
[d] Estimations from $\bar{M}_{F160W}$.

stellar population (Ferreras, Charlot, & Silk 1999). For all these reasons the comparison between our predictions for t and Z, and those obtained using other methods have to be considered with caution, and within the quoted approximations. The age and metallicity we derive have large uncertainties, as expected from the quoted limitations. A more detailed investigation is beyond the aim of this paper and should rely on mixed population models, as well as SBF measurements for which the radial distribution is known (e.g., Sodemann & Thomsen 1995).

In order to test our ability to predict age and metallicity, we built a sample of 15 galaxies for which these quantities have been determined by other authors (Table 9). Most of these objects come from the compilations of TFWG00 and Terlevich & Forbes (2002, hereafter TF02), who used Hβ, Mg b, and $\langle$Fe$\rangle$ line strengths to derive age and metallicity for a large sample of elliptical galaxies (see the quoted papers for more details). These estimations are derived from observational data taken at smaller radii with respect to SBF measurements (except in the case of Jensen et al. 2001, 2003). In addition, TFWG00 find indications of age and metallicity gradients (see their Tables 6A and 6B).

To start with, let us use the model sequences in the $\bar{M}_X$ versus $(V-I)_0$ plane as already shown in Figures 14 and 15. The clear separation between models with low ($Z = 0.0001,\ 0.001$) and high ($Z = 0.01,\ 0.02,\ 0.04$) metallicity for all the explored values of age confirms that this kind of diagram is a powerful tool for this purpose (see also BVA01; LCG00). Since we are dealing with absolute SBF amplitudes, particular care has to be taken in selecting the DMs required to translate the observed apparent SBF values. Obviously, Cepheid distances are preferred; when they are not available for a single galaxy, we use group-averaged distances. To avoid circular arguments, we recomputed the group DMs by Ferrarese et al. (2000), excluding SBF-derived distances, i.e., averaging over the Cepheids, planetary nebula luminosity function (PNLF), and the RGB-tip distances. The results are reported in Table 9 for the 15 galaxies. As already stated, Freedman et al. (2001) revised the Cepheid distance scale, and Ciardullo et al. (2002) recently recalibrated the zero point of the PNLF. These new results decrease the group-averaged distances by about 0.14 mag if the Cepheid PL relation is used, but they leave nearly unchanged the above determinations when the PLZ relation is considered.

Figure 16 displays the theoretical models and the observational data in selected photometric bands. As a first general result, we find that the location of the bulk of the galaxies is almost consistent in all the photometric bands. We next focus on two well-studied galaxies: NGC 224 (M31) and its dwarf companion NGC 221 (M32). They have accurate distances and different morphological types, and thus they are good prototypes for our investigation.

NGC 221.—The observed V-, I-, K-, and F160W-band SBFs are well reproduced by SSP models with an age between 5 and 9 Gyr and a nearly solar chemical content. These results are very similar to those found by TFWG00 and TF02, i.e., $t = 4.9 \pm 1.3$ Gyr with $[Fe/H] = -0.01 \pm 0.05$, and $t = 3.8$ Gyr with $[Fe/H] = -0.04$, respectively.

NGC 224.—The V-, I-, and F160W-band SBF data for the bulge of this galaxy are consistent with SSP models of fairly old age ($t \sim 5$ Gyr) and solar metallicity. This is in agreement with Bica, Alloin, & Schmidt (1990) and Davidge (2001), who find that the bulge of this galaxy is dominated by an old population with metal content $-0.5 < \log(Z/Z_\odot) < 0.0$. There is a discrepancy with the age estimation ($t \sim 5$ Gyr) of TF02. However, Davidge (1997) finds evidence for an age gradient in the center of NGC 224, with an intermediate-age population that is probably more concentrated in the center with respect to the main body of the bulge; such a population should contribute only a small fraction (10%–20%) to the total visible flux.

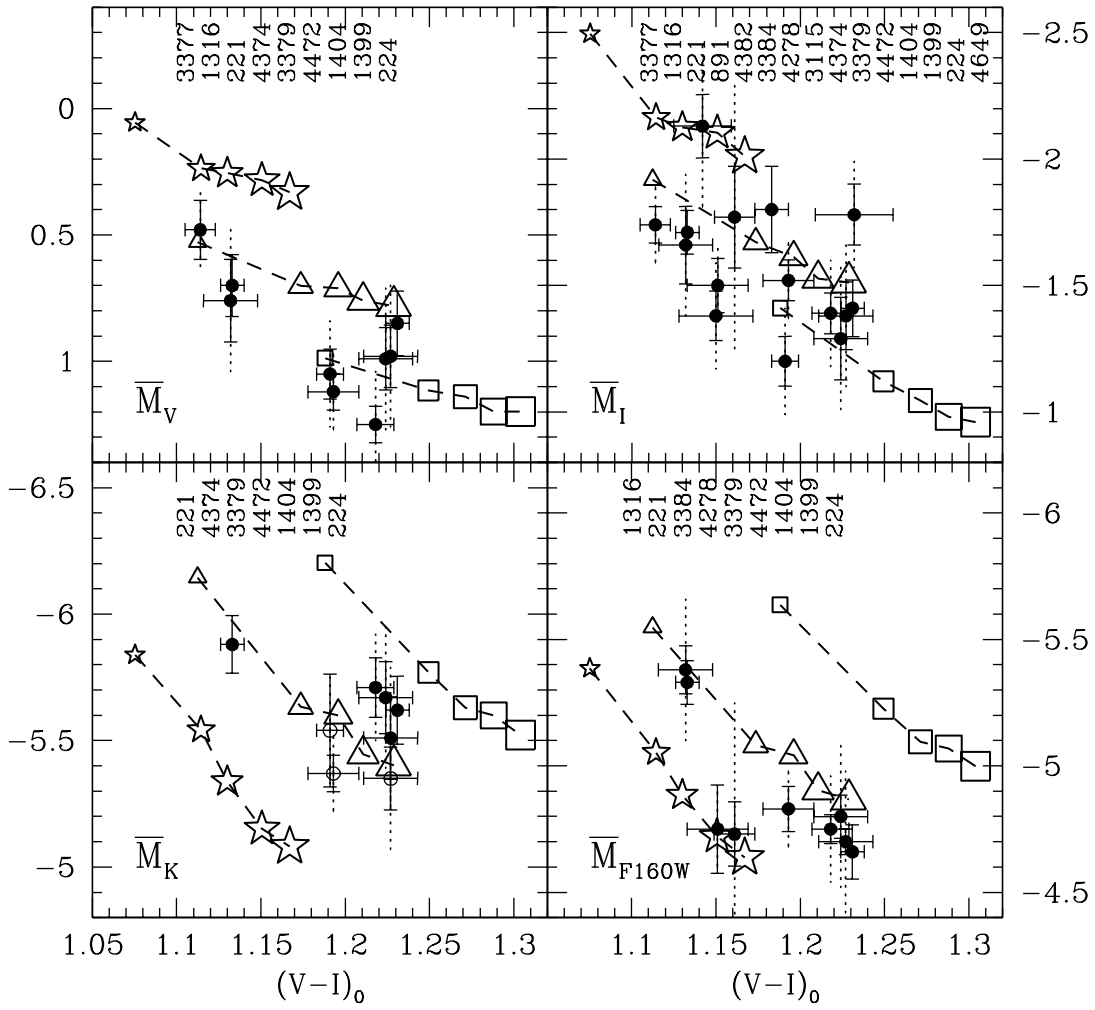

FIG. 16.—Subsample of galaxies with age and metallicity estimations from the literature, plotted against theoretical models for all ages and metallicity higher than half-solar. The galaxies are identified at the top of each panel according to increasing integrated $(V-I)_0$ color. For each galaxy we also report the size of the depth of its group according to Ferrarese et al. (2000; *vertical dotted line*).

It is difficult to derive information from the *K*-band SBFs, because of the previously mentioned overlap of models. However, the $\bar{M}_K$ data are consistent with the (t, Z)-values inferred from *V*- and *I*-band estimations. Some remarkable indications from NIR data can be found by comparing the SSP models, which reproduce the *V*- and *I*-band SBFs, with the work by Davidge (2001). Observing the brightest AGB stars in the M31 bulge, Davidge finds that the bulk of these stars have $K \simeq -8.4$ mag. By adopting in our SSP models ($t = 15$ Gyr, $Z = 1\ Z_\odot$) the mass-loss calibration suggested in § 4.2.2 (i.e., $\eta_{\rm AGB} = 0.8$), we find that the tip of the AGB is as bright as $K \simeq -8.2$ mag, a value that is in very good agreement with the observational results of Davidge.

Among the other galaxies, there are some examples that support the consistency of our estimates in the various bands and that are concordant with values proposed in the literature (see Table 9):

NGC 891.—The most metal-poor galaxy in our sample, we derive $Z \sim \frac{1}{2}\ Z_\odot$ and age 11–13 Gyr.

NGC 1316.—The *V*, *I*, and F160W SBF magnitudes suggest a young age ($t \sim 5$ Gyr) and a nearly solar metallicity.

NGC 3377.—The *V*- and *I*-band SBF measurements appear to be consistent with a nearly solar composition and relatively young age (∼5 Gyr)

NGC 3379.—An age on the order of 11–13 Gyr and a solar chemical composition are derived from the SBF measurements in two bands (*K* and F160W). On the other hand, *V*- and *I*-band SBF data would require a somewhat younger age (∼5–9 Gyr) and a higher metallicity ($Z > Z_\odot$). This discrepancy should disappear below with the use of SBF color data.

NGC 4382.—Only SBF measurements in the *I*-band are available, and this galaxy seems to be located slightly out of the model grid, in the area of the diagram where we expect to find stellar systems with $Z \gtrsim 2\ Z_\odot$ and an age younger than 5 Gyr.

NGC 4472.—The *I*- and F160W-band SBF measurements are in agreement with an SSP computed assuming $Z = 1\ Z_\odot$ and an old age (∼15 Gyr), while a slightly higher metallicity and lower age are suggested by the *V* and *K* bands.

For some galaxies the slight discrepancies in the values derived from different bands could be related to the high uncertainty of their DMs, coupled with a different sensitiv-

ity of the SBFs in each band to age and metallicity. Concerning distances, we mention also the case of the galaxy NGC 4649, which is located outside of the grid of models in the $\bar{M}_I$ panel. As discussed by Ferrarese et al. (2000), the NGC 4649 Virgo subcluster is not a well-defined physical association of galaxies; thus, the group distance reported in Table 9 is probably not an appropriate choice for the actual distance of the galaxy. A direct measure of the distance of NGC 4649 comes from the PNLF; if we adopt this value, the inferred age and metallicity are estimated to be $t \sim 5$–9 Gyr and $Z = 2\ Z_{\odot}$. However, we recall Jacoby et al.'s (1992) and, recently, Ciardullo et al.'s (2002) remarks that the PNLF distances seem to be systematically shorter than SBF distances. For this reason, we do not report these estimates in Table 9.

We find a discrepancy in the age and metallicity derived from $\bar{M}_I$ and $\bar{M}_{\rm F160W}$ for NGC 4278 and NGC 3384. For NGC 4278, the situation is similar to that of NGC 4649; for NGC 3384, such a discrepancy could be related to the multicomponent structure of this galaxy (Busarello et al. 1996), coupled with the fact that *HST* SBF measurements refer to the very inner region of the galaxy, while an outer region was observed by T01.

The above results are summarized in Table 9 (cols. [7]–[8]). Clearly, the comparison with the evaluations of TFWG00 and TF02 should not be overinterpreted; nonetheless, the fair agreement obtained is remarkable and supports the reliability of our models.

Although the $\bar{M}_X$ versus $(V-I)_0$ planes can be used to set useful (though not stringent) constraints on the evolutionary properties of the main stellar population present in a galaxy, the drawback is mainly the dependence on the adopted distance and on the partial degeneracy between age and chemical composition found at higher metallicity ($Z \geq 0.01$). To solve this ambiguity, *SBF color* versus *integrated color* diagrams are useful, since they appear to be strongly dependent on stellar population properties (age and metallicity), and even more remarkably, neither quantity depends on distance determinations.

To quantify this theoretical expectation, in Figure 17 we plot the selected theoretical SBF color (involving *VIHK* bands) versus the theoretical integrated color $(V-I)_0$. Theory predicts up to a 3.5 mag difference in $\bar{M}_V-\bar{M}_K$ for populations with extreme Z-values, and nearly 3 mag in $\bar{M}_I-\bar{M}_K$. Therefore, for stellar population analysis, it would be of the greatest interest to gain SBF measurements to derive the $\bar{M}_V-\bar{M}_K$ color.

In Figures 18 and 19, observational data are compared with the theoretical SBF models in the $(\bar{M}_V-\bar{M}_I)$-$(V-I)_0$

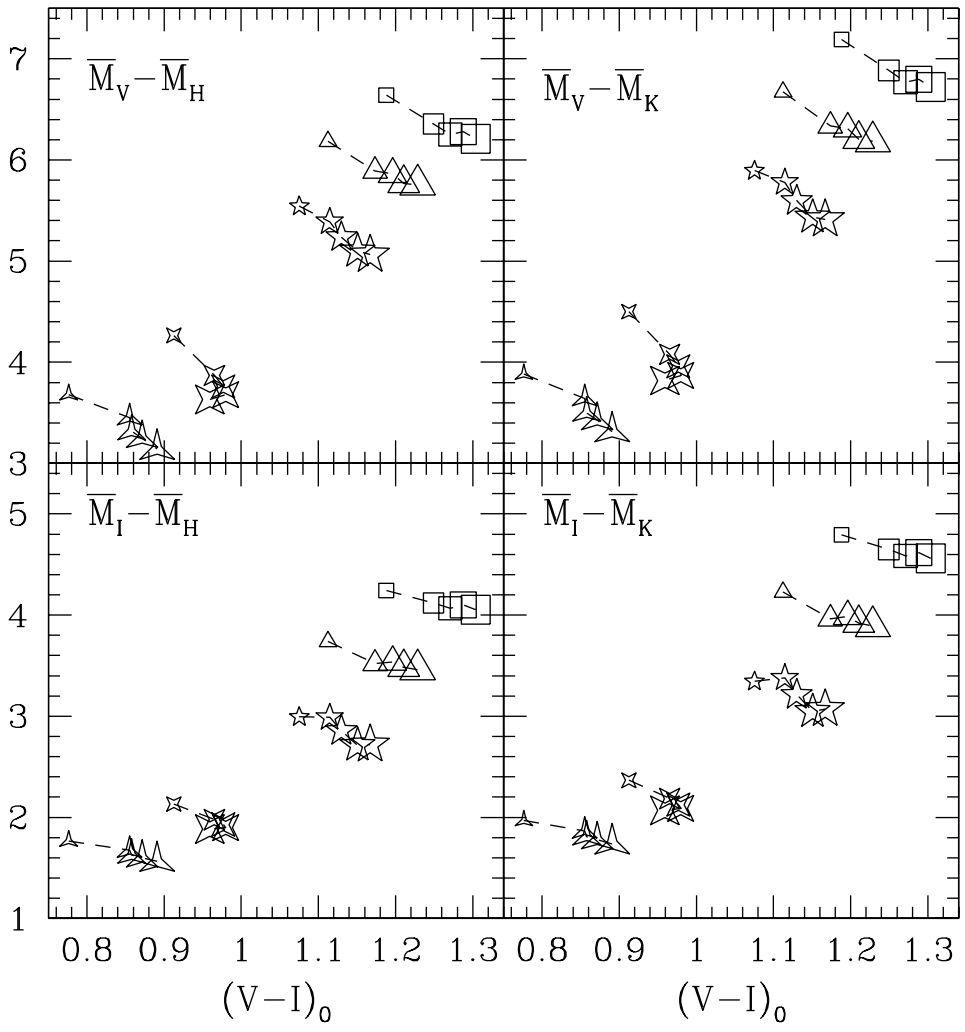

FIG. 17.—Theoretical SBF color vs. integrated $(V-I)_0$ color diagrams obtained with our fluctuation models. Note the major excursion of $\bar{M}_V-\bar{M}_K$ color for extreme Z-values, compared with other SBF colors. (Symbols are as in Fig. 8.)

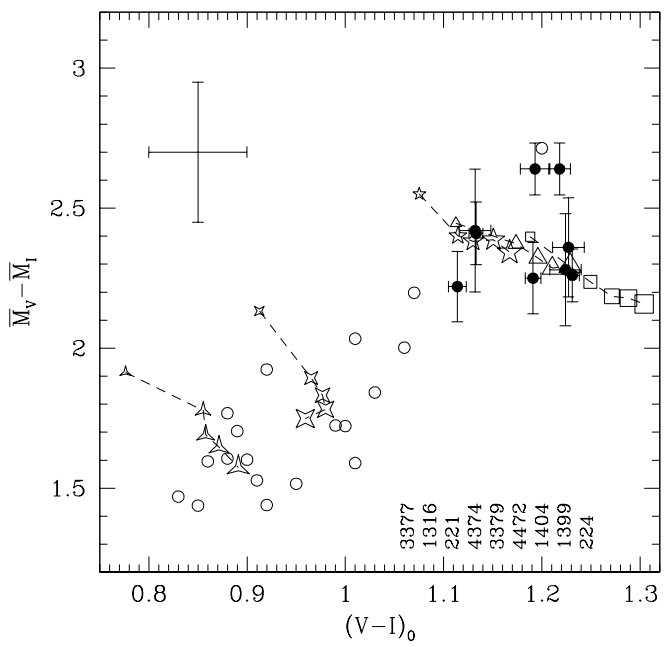

FIG. 18.—The $\bar{M}_V-\bar{M}_I$ color plotted against the integrated color $(V-I)_0$. Open circles refer to GGC data, and filled circles refer to galaxies. The typical error bars of GGC data are also plotted.

and $(\bar{M}_I-\bar{M}_K)$-$(V-I)_0$ planes. In both figures the bulk of the galaxies are clearly concentrated near the position of the SSP having solar chemical composition and ages greater than 10 Gyr, i.e., the expected locus for early-type galaxies.

The models in Figure 18 are again sharply divided into two regions that identify different ranges of metallicity. This feature is substantiated by the location of the observational data: GGCs, which occupy the low-metallicity portion, and galaxies, at redder $(V-I)_0$. As age increases, we expect a redder $(V-I)$ and bluer $\bar{M}_V-\bar{M}_I$, confirming the results of BVA01.

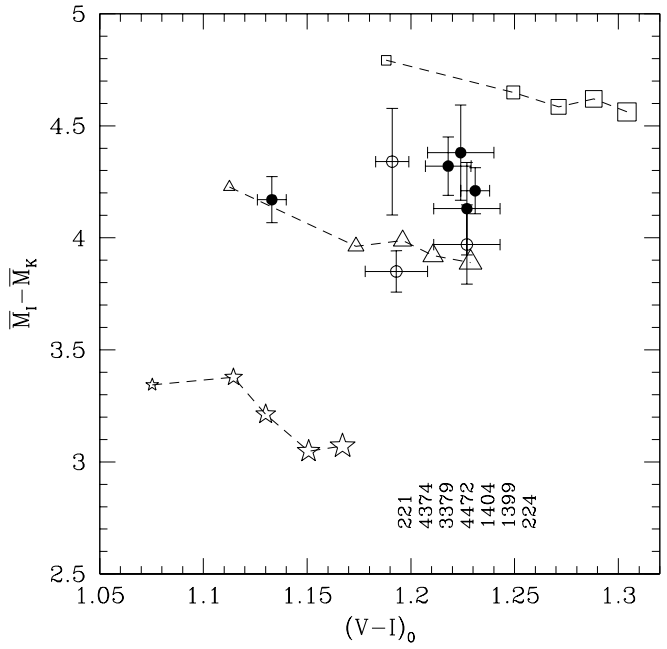

FIG. 19.—The $\bar{M}_V-\bar{M}_K$ color vs. the integrated color $(V-I)_0$. For clarity we only plot the models with the highest metallicity considered.

As tracer of stellar population features, $\bar{M}_V-\bar{M}_I$ is not particularly accurate, because of the superposition of models with $0.01 \leq Z \leq 0.04$ clearly seen in Figure 18. To disentangle the age-metallicity degeneracy, a better choice of SBF colors should be made. For example, $\bar{M}_I-\bar{M}_K$ and $\bar{M}_V-\bar{M}_K$ are preferred. Concerning the $(\bar{M}_I-\bar{M}_K)$ color, Figure 19 shows that the separation between models with different chemical composition is high enough to allow an evaluation of metallicity despite the nonnegligible mean error of the observed SBF color. In particular, by adopting this kind of diagram the ambiguity shown in the *K*-band SBFs (Fig. 16) for some galaxies can be resolved. For instance, NGC 224's properties are now derived by simple interpolation of the SBF models. Similarly to NGC 224, we can take advantage of this diagram, and the age-metallicity degeneracy is fairly removed for several other galaxies. In Table 9 (cols. [9] and [10]) we summarize the results, reporting the age and metallicity values inferred from the location of the SBF measurements of each given galaxy in the $(\bar{M}_I-\bar{M}_K)$-$(V-I)_0$ plane.

One may note that the fair agreement found between the results in columns (7)–(9) and (8)–(10) in Table 9 supports the general consistency of the two SBF methods. However, a few galaxies show some differences. This is not surprising, because several sources of uncertainty are at work in a differential way in the two methods. Let us recall few of them: (1) the distance moduli, (2) the presence of secondary populations, and (3) the reddening. Each of these requires evaluations or assumptions that affect the location of the observational points in the two diagrams.

Before concluding this section, let us emphasize that all our results come from single-burst stellar population models. On this point, we recall that by comparing their models with observations in the $\bar{M}_I-\bar{M}_K$ versus $\bar{M}_V-\bar{M}_I$ plane,

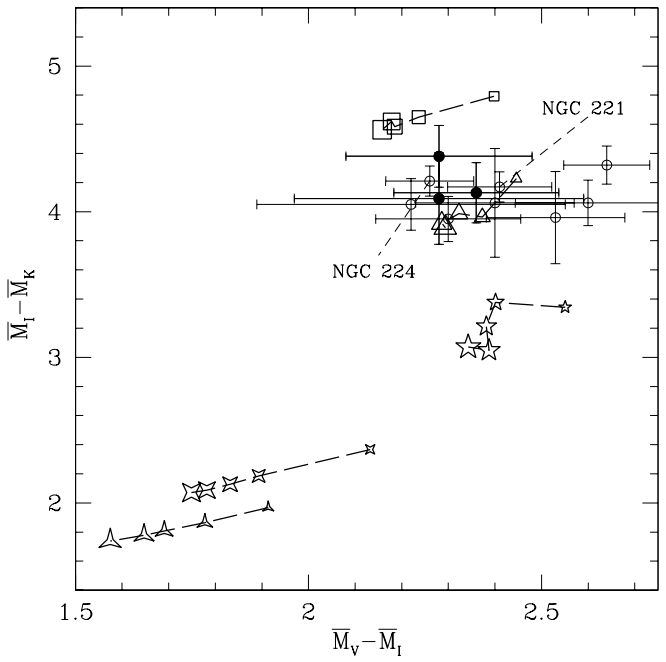

FIG. 20.—The $\bar{M}_V-\bar{M}_I$ color plotted vs. the $\bar{M}_V-\bar{M}_K$ for the new models (symbols as in Fig. 8) and observational data. The observed SBF amplitudes of galaxies are *V*-band from BVA01 (*filled circles*), TAL90 (*open circles*), and AT94 (NGC 224); *I* band from T01; *K* band from Luppino & Tonry (1993) and Jensen, Tonry, & Luppino (1998).

BVA01 conclude that composite stellar populations appear necessary for those galaxies with $\bar{M}_V - \bar{M}_I \leq 2.3$. On the other hand, the present models for simple stellar populations seem to match, at least within the observational uncertainties, the locus of the available measurements (see Fig. 20); in particular, the two Local Group galaxies NGC 221 and NGC 224 are well fitted. Of course, in order to better reproduce the SBFs of each individual galaxy (for example, the galaxy with the highest $\bar{M}_V - \bar{M}_I$, NGC 4472), it could be useful to introduce composite stellar populations, even if this implies adopting ad hoc scenarios (see BVA01).

6. USEFUL RELATIONS

In accord with the foregoing discussion, the single-burst models proposed in this work can be reliably adopted for both distance estimations and stellar population analysis. Some useful expressions can be given to obtain a straightforward determination of the SBF magnitudes once the integrated $(V-I)_0$ color of a galaxy has been measured. The least-squares method applied to theoretical models with ages $t \geq 9$ Gyr and metallicity $Z \geq 0.001$ [equivalently, $(V-I)_0 \geq 0.95$] provides

$$\bar{M}_V = (0.43 \pm 0.10) + (5.26 \pm 0.22)[(V-I)_0 - 1.15] , \quad (2)$$

$$\bar{M}_R = (-0.52 \pm 0.14) + (5.37 \pm 0.31)[(V-I)_0 - 1.15] , \quad (3)$$

$$\bar{M}_I = (-1.74 \pm 0.23) + (3.93 \pm 0.50)[(V-I)_0 - 1.15] , \quad (4)$$

$$\bar{M}_K = (-5.22 \pm 0.23) - (3.87 \pm 0.50)[(V-I)_0 - 1.15] . \quad (5)$$

The relations presented here show a very good agreement for both V and I bands with the empirical calibrations of T01 and BVA01. The calibration of the R band is fairly similar to that presented by BVA01.

Concerning the $\bar{M}_K$ calibration, it appears quite different from the empirical result of LGC02. In particular, the theoretical calibration predicts an opposite trend with respect to the empirical one. This behavior has been discussed by LGC02; here we point out that the age of the observed stellar population may play a relevant role. In fact, Figure 15*b* shows an age dependence of the K-band SBF amplitudes that is much larger than those expected in V and I (Fig. 15*a* and Fig. 14). More complex models (e.g., LGC02) and further observations in the K band are required in order to clarify this discrepancy. A similar result is obtained for $\bar{M}_{\rm F160W}$ when the calibration is compared with the empirical one recently found by Jensen et al. (2003). Thus, the fact that NIR SBF age and metallicity variations have no degenerate effects makes it quite problematic to derive accurate one-parameter SBF calibrations for these wavelengths.

In conclusion, the theoretical $\bar{M}_X$ versus $(V-I)_0$ relations agree well (except for NIR filters) with the empirical relations, even in the simple adopted scenario of single-burst populations.

7. CONCLUSIONS

In this paper we have developed a new theoretical model for SBF predictions of simple stellar populations (single burst, single chemical composition) with ages ranging from 5 to 15 Gyr, and metallicity from 1/200 to 2 $Z_\odot$, relative to the standard *UBVRIJHK* ground-based filters and the F439W, F555W, F814W, F110W, F160W, and F222M of the *HST* photometric system (WFPC2 and NICMOS). The model relies on the stellar population synthesis code developed by Brocato et al. (2000), optimized for a fine simulation of the latest (brightest) phases of stellar evolution, which have a strong influence on SBF magnitudes.

The procedure adopted to compute the SBF amplitudes is different from previous theoretical works, and it has the advantage of being quite similar to the observational approach currently used to measure the pixel-to-pixel fluctuations in real galaxies. With this tool we simulated the effect of the mass-loss processes along the RGB, the AGB, and the thermal pulse phase. In particular, the impact of mass loss on the prediction of SBF magnitudes has been investigated, with the finding that a careful treatment of this quantity is fundamental to determining reliable SBF evaluations.

Following the formalism of Reimers (1975), we adopted $\eta_{\rm RGB} = 0.4$ for RGB stars. An independent calibration of the efficiency of mass loss along the AGB was performed by using the SBF technique. A set of models with different assumptions for $\eta_{\rm AGB}$ was computed. The observed SBF measurements of GGCs and galaxies efficiently constrain the theoretical expectations, showing that the data are well reproduced by SSPs of the proper age and metallicity if $\eta_{\rm AGB} = 0.8$. Such values agree well with observational data (Le Bertre et al. 2001) and impressively reproduce the absolute K-band magnitude of the stars at the tip of the AGB in NGC 224. To our knowledge, this is the first time that SBF measurements have been used to constrain stellar evolution models of AGB stars. We also compared our models with previous works (BVA01; LCG02), finding a substantial general agreement, despite the different stellar evolution models adopted in the computations of the SSPs that generate the SBF evaluations.

The impact on SBFs of assumptions regarding the IMF have been investigated and quantified by the adoption of a set of reasonable values for the exponent of a Scalo-like mass distribution. The consequences of cutting the IMF at a low-mass limit are also presented. As expected, the contribution of the upper part of the MS cannot be neglected.

We investigated the effects of different assumptions regarding the relation to transform theoretical quantities [$\log (L/L_\odot)$ and $\log T_{\rm eff}$] into observed magnitudes and colors on SBF predictions. We found that the compilations of Green et al. (1987), Castelli et al. (1997), and Lejune et al. (1997) provide quite similar SBF predictions for models with $Z < 0.01$, while sizable differences should be expected if SSPs of high Z are involved.

Once the theoretical framework defining the SSP models was fixed, we successfully checked the capability of deriving distances from our SBF predictions. This was done for a sample of GGCs for which SBF measurements are available and with a sample of properly selected galaxies of known distances.

As a result, a set of calibrations of absolute SBF magnitudes for classical *UBVRIJHK* photometric bands and for selected *HST* filters is provided. Tests with other distance indicators (Cepheids, the PNLF, SBF empirical relations, etc.) show that the degree of accuracy and precision of the present theoretical calibration of the absolute SBF magnitudes is sufficient to justify the use of these theoretical SBFs as a *primary distance indicator*.

On the other side, we tested the use of SBFs as tracers of stellar population properties. In particular, we derived ages and metallicities for a subsample of galaxies for which SBF observations and reliable distances are available. The results appear very promising, since the obtained values are comparable to evaluations derived by other methods. Moreover, *SBF color* versus *integrated color* diagrams are proposed to be particularly useful in removing the well-known age-metallicity degeneracy (e.g., Worthey 1994), which affects our knowledge of remote stellar systems.

Finally, we suggest that future observations should take advantage of the high sensitivity of SBF measurements as stellar population tracers on the blue side of the spectral energy distribution of galaxies. This would be a meaningful scientific target for ground-based telescopes with high efficiency in the *B* wavelength range (VLT Survey Telescope) or for telescopes located out of the Earth's atmosphere (*HST* and the *James Webb Space Telescope*).

Financial support for this work was provided by MIUR-Cofin 2000, under the scientific project "Stellar Observables of Cosmological Relevance." This project made use of computational resources granted by the Consorzio di Ricerca del Gran Sasso according to Progetto 6, Calcolo Evoluto e sue Applicazioni (RSV6), Cluster C11/B. We thank the anonymous referee for a careful reading of the manuscript and for several useful suggestions for clarifying the presentation; the constructive report helped us to improve the paper.

APPENDIX

THE PROCEDURE

For the sake of clarity, we outline here the major steps of the procedure we have adopted to derive SBF magnitudes. As a first step, one needs to evaluate the total flux emitted by a stellar population generated by a single burst of star formation. In our model we make the assumption that the integrated light is dominated by the emission generated by stars of the simulated stellar system. This implies that (1) no sources of nonthermal emission are at work, (2) the thermal emission by interstellar gas makes no sizable contribution to the integrated flux, and (3) the absorption from dust and gas is negligible. On this basis, the integrated flux in a selected photometric filter X can be obtained by knowing two quantities,

$$f_X(L(m, t, Y, Z), T_{\rm eff}(m, t, Y, Z), Y, Z) , \quad \Phi(m, N) ,$$

where f_X is the flux emitted by a star of mass m, age t (stellar system age), luminosity L, effective temperature $T_{\rm eff}$, and chemical composition (Y, Z). Obviously, f_X is defined by an extended library of homogeneous and self-consistent stellar evolutionary tracks (see § 2), but it also depends on the adopted transformation tables (see § 4.3).

The second quantity, Φ, is strictly related to the IMF and represents the number of stars with mass m in a population globally constituted of N stars, with age t and chemical composition (Y, Z). A fundamental point is that the distribution of star masses along the IMF is obtained by using a Monte Carlo method. Special attention was paid to ensure that when a set of simulations with the same input parameters is computed, each distribution is fully independent of the previous extractions.

Both the quantities are properly combined and integrated by the stellar population code to derive the total integrated flux F_X of the simulated stellar system in the selected photometric band:

$$F_X(N, t, Y, Z) = \sum_{i=1}^{N} f_X^i \ ; \tag{A1}$$

thus, this quantity evaluates the absolute integrated flux of a stellar population of N stars with age t, chemical composition (Y, Z), and a given IMF, as located at the reference distance of 10 pc.

If a number $N^*_{\rm sim}$ of simulations with exactly the same input parameters are computed, the resulting $F^j_X(N, t, Y, Z)$ are *not* expected to be constant, since the initial mass distribution of each simulation is randomly generated. Thus, even if we adopt the same IMF law, each jth mass distribution is fully independent from previous extractions. As a consequence, the resulting distribution of the stars in the CMD changes. In particular, the bright stars on the RGB and AGB (i.e., the most relevant contributors to the integrated light) are expected to undergo sizable variations in number and CMD position, and this qualitatively explains the fluctuations F_X.

In principle, this can be considered quite similar to what happens in observing an ideal galaxy in which the same population is spread over a number of pixels. Under the assumption of an ideal galaxy constituted of a homogeneous stellar population, the number and the luminosity of bright stars may change from pixel to pixel, again from Poisson statistical fluctuations. Thus, the measured flux in each pixel is expected to be affected by the fluctuations (TS88).

By following the formalism of Tonry and collaborators, we consider the amplitude of the expected fluctuations (SBFs) $\bar{F}_X$ as the ratio of the variance to the average integrated flux, i.e.,

$$\bar{F}_X \equiv \frac{\langle F_X - \langle F_X \rangle^2 \rangle}{\langle F_X \rangle} = \frac{\sum_j (F^j_X - \langle F_X \rangle)^2}{N^*_{\rm sim} - 1} \frac{1}{\langle F_X \rangle} \ , \tag{A2}$$

where the average flux $\langle F_X \rangle$ of the selected population is given by

$$\langle F_X \rangle = \frac{\sum_j F^j_X}{N^*_{\rm sim}} \ . \tag{A3}$$

From the operational point of view, for each set of parameters (age, chemical composition, IMF, etc.), which identifies a stellar population model, we compute a large number of independent simulations ($N^*_{\rm sim} = 5000$) deriving the F^j_X for each model. At this point the SBF flux is computed directly, using the right-hand side of equation (A2) and the definition from equation (A3). Finally, the SBF flux is converted into the SBF magnitude $\bar{M}_X$ in the usual way,

$$\bar{M}_X = -2.5 \log \bar{F}_X \ . \tag{A4}$$

In order to compare our method for computing SBFs with those obtained by applying the "usual" procedure (i.e., to integrate the luminosity function times the squared

TABLE A1

SBF Predictions for a Stellar Population with $t = 15$ Gyr and $1\ Z = Z_{\odot}$ as a Function of Total Number of Stars

$N_{\rm star}$	$V_{\rm tot}$	$\bar{M}_B$	$\bar{M}_V$	$\bar{M}_I$	$\bar{M}_K$	$(V-I)_0$
10^3	0.455	2.236	0.710	−1.551	−5.373	1.055
10^4	−2.292	2.365	0.795	−1.504	−5.408	1.192
10^5	−4.822	2.353	0.781	−1.513	−5.402	1.233
10^6	−7.325	2.407	0.839	−1.473	−5.403	1.235
5×10^6.....	−9.074	2.395	0.831	−1.483	−5.410	1.235
2.6×10^7.....	−10.847	2.469	0.910	−1.474	−5.414	1.235
2.1×10^8.....	−13.098	2.589	0.989	−1.391	−5.365	1.235
Usual	...	2.599	1.040	−1.371	−5.381	...

flux per luminosity bin and divide by the total flux; see, e.g., TS88; BVA01), we directly computed the SBF values for several input parameters by using both our method and the usual one. To provide a quantitative example, we report in Table A1 the results for stellar population models with $t = 15$ Gyr and $Z = 1\ Z_{\odot}$.

The procedure outlined here gives SBF amplitudes that are in agreement with those obtained from the usual method when the number of stars ($N_{\rm star}$) in each simulation is so large that all the brightest bins in the luminosity function have a number of stars greater than zero. The condition for full equivalence of the two methods is satisfied when the limit of large numbers is approached (TS88). We find that this limit is reached when $N_{\rm star} \gtrsim 10^8$ (in the mass interval $0.1\ M_{\odot} \leq M \leq 1.5\ M_{\odot}$), because the probability of finding very bright stars in each simulation becomes high enough. As $N_{\rm star}$ decreases, the differences between the SBF values computed by the two methods increase.

Although the procedure outlined in this work is not particularly efficient in terms of computational time, it has some advantages. One point is that our approach to deriving SBF amplitudes is closer to the observational method of measuring SBFs in real galaxies. In fact, the opportunity of generating $N_{\rm sim}$ for independent stellar populations, each of which includes $N_{\rm star}$ stars, closely resembles what is directly measured in $N_{\rm sim}$ pixels of a galaxy CCD image (neglecting seeing effects), where a single pixel contains $N_{\rm star}$ stars. Here we have typically adopted $N_{\rm star} = 10^5$, which may represent the estimated number of stars per pixel for a galaxy in the Virgo Cluster observed with a CCD having $0\farcs3$ pixel^{-1} (§ 2). For such an assumption, the limit of large numbers is not satisfied. This implies a relatively small shift between the SBF amplitudes obtained with our procedure and those obtained with the usual one, as shown in Table A1 (Fig. 21).

As an interesting new result, we suggest that the SBF magnitudes appear to have a small but nonnegligible dependence on the population (pixel) star density. Although this dependence is only a second-order correction, it should be further investigated, both on the theoretical and the observational side, for a deeper understanding and refining

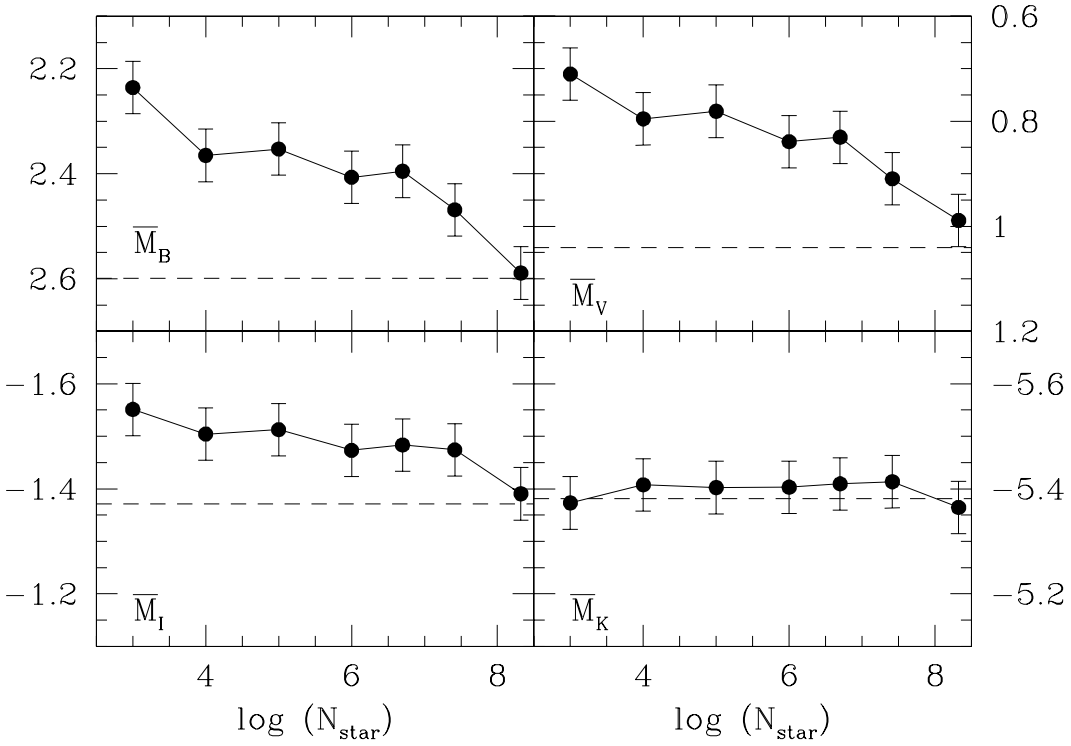

Fig. 21.—SBF amplitudes obtained with the "usual" method (*dashed lines*) and the present work (*circles*) vs. log $N_{\rm star}$

of the SBF method. In particular, we suggest that the present approach would be useful when dealing with SBF measurements obtained by pixels in which the expected number of stars is relatively low (nearby galaxies, high-resolution telescopes, loose galaxies) when compared with typical observations in elliptical galaxies.

As a final consideration on the capability of our way of computing SBFs we note that it is also particularly efficient in handling the details of all the stellar evolutionary phases. In fact, each independent stellar population is computed by leaving to the statistics the possibility of distributing stars in the CMDs according to their proper evolutionary pattern. On the other hand, the usual way makes use of predefined isochrones, which fix, by definition, one single pattern in the CMD (i.e., a fixed luminosity function) for each set of input parameters (t, Z). A relevant example is the distribution of horizontal-branch stars. As previously shown by Rood et al. (1973), the HB morphology can hardly be described by uniparametric (mass) curves, as assumed when dealing with isochrones. In our procedure we always compute a synthetic HB that reproduces the color spread and relative star counts observed in real HBs (Brocato et al. 2000). Moreover, isochrones are generally computed by assuming a fixed value for the mass-loss rate along the RGB. On the other hand, in the present stellar population synthesis code the mass loss and its spread around an average value can be chosen as free input parameters (§ 4.2.1).

REFERENCES

Ajhar, E. A., Lauer, T. R., Tonry, J. L., Blakeslee, J. P., Dressler, A., Holtzman, J. A., & Postman, M. 1997, AJ, 114, 626
Ajhar, E. A., & Tonry, J. L. 1994, ApJ, 429, 557 (AT94)
Alard, C., et al. 2001, ApJ, 552, 289
Alonso, A., Arribas, S., & Martínez-Roger, C. 1996, A&AS, 117, 227
———. 1999, A&AS, 140, 261
Baugh, C. M., Cole, S., & Frenk, C. S. 1996, MNRAS, 283, 1361
Bell, R. A. 1973, MNRAS, 164, 197
Benedict, G., et al. 2002, AJ, 123, 473
Bertelli, G., Bressan, A., Chiosi, C., Fagotto, F., & Nasi, E. 1994, A&AS, 106, 275
Bessel, M. S. 1979, PASP, 91, 589
Bica, E., Alloin, D., & Schmidt, A. A. 1990, A&A, 228, 23
Blakeslee, J. P., Ajhar, E. A., & Tonry J. L. 1999, in Post-*Hipparcos* Cosmic Candles, ed. A. Heck & F. Caputo (Dordrecht: Kluwer), 181
Blakeslee, J. P., Vazdekis, A., & Ajhar, E. A. 2001, MNRAS, 320, 193 (BVA01)
Blöcker, T., & Schönberner, D. 1997, A&A, 324, 991 (BS97)
Bono, G., Caputo, F., Cassisi, S., Castellani, V., & Marconi, M. 1997a, ApJ, 479, 279
———. 1997b, ApJ, 489, 822
Bressan, A., Chiosi, C., & Tantalo, R. 1996, A&A, 311, 425
Brocato, E., Capaccioli, M., & Condelli, M. 1998, Mem. Soc. Astron. Italiana, 69, 155
Brocato, E., Castellani, V., Poli, F.M., & Raimondo, G. 2000, A&AS, 146, 91 (BCPR00)
Brocato, E., Castellani, V., Raimondo, G., & Romaniello, M. 1999, A&AS, 136, 65
Brocato, E., Matteucci, F., Mazzitelli, I., & Tornambé, A. 1990, ApJ, 349, 458
Busarello, G., Capaccioli, M., D'Onofrio, M., Longo, G., Richter, G., & Zaggia, S. 1996, A&A, 314, 32
Buzzoni, A. 1993, A&A, 275, 433 (B93)
Cantiello, M. 2001, Ph.D. thesis, Univ. Napoli
Carollo, C. M., Danziger, I. J., & Buson, L. 1993, MNRAS, 265, 553
Cassisi, S., Castellani, V., degl'Innocenti, S., & Weiss, A. 1998, A&AS, 129, 267
Castellani, V., Chieffi, A., & Pulone, L. 1991, ApJS, 76, 911
Castellani, V., Chieffi, S., & Straniero, O. 1992, ApJS, 78, 517
Castellani, V., & Tornambé, A. 1991, ApJ, 381, 393
Castelli, F., Gratton, R. G., & Kurucz, R. L. 1997, A&A, 318, 841 (CGK97)
Ciardullo, R., Feldmeier, J. J., Jacoby, G. H., Kuzio de Naray, R., Laychak, M. B., & Durrell, P. R. 2002, ApJ, 577, 31
Cousins, A. W. J. 1976, MmRAS, 81, 25
———. 1978, Mon. Notes Astron. Soc. South Africa, 37, 8
Davidge, T. J. 1997, AJ, 113, 985
———. 2001, AJ, 122, 1386
Ferrarese, L., et al. 2000, ApJS, 128, 431
Ferreras, I., Charlot, S., & Silk, J. 1999, ApJ, 521, 81
Freedman, W. L., et al. 2001, ApJ, 553, 47
Freeman, K. C., & Norris J. 1981, ARA&A, 19, 319
Girardi, L., Bressan, A., Bertelli, G., & Chiosi, C. 2000, A&AS, 141, 137
Green, E. M., Demarque, P., & King, C. R. 1987, in The Revised Yale Isochrones and Luminosity Functions (New Haven: Yale Univ. Obs.) (GDK87)
Greggio, L., & Renzini, A. 1990, ApJ, 364, 35
Groenewegen, M. A. T., & de Jong, T. 1993, A&A, 267, 410
Harris, W. E. 1996, AJ, 112, 1487
Henry, R. B. C., & Worthey, G. 1999, PASP, 111, 919
Jacoby, G. H., et al. 1992, PASP, 104, 599
Jensen, J. B., Luppino, G. A., & Tonry, J. L. 1996, ApJ, 468, 519
Jensen, J. B., Tonry, J. L., Barris, B. J., Thompson, R. I., Liu, M. C., Rieke, M. J., Ajhar, E. A., & Blakeslee, J. P. 2003, ApJ, 583, 712
Jensen, J. B., Tonry, J. L., & Luppino, G. A. 1998, ApJ, 510, 71
Jensen, J. B., Tonry, J. L., Thompson, R. I., Ajhar, E. A., Lauer, T. R., Rieke, M. J., Postman, M., & Liu, M. C. 2001, ApJ, 550, 503
Jerjen, H., Binggeli, B., & Freeman, K. C. 2000, AJ, 119, 593
Jerjen, H., Freeman, K. C., & Binggeli, B. 1998, AJ, 116, 2873
Jerjen, H., Rekola, R., Takalo, L., Coleman, M., & Valtonen, M. 2001, A&A, 380, 90
Johnson, H. L., & Morgan, W. W. 1953, ApJ, 117, 313
Kauffmann, G., & Charlot, S. 1998, MNRAS, 294, 705
Kobayashi, C., & Arimoto, N. 1999, ApJ, 527, 573
Kudriztki, R.-P., Pauldrach, A., & Puls, J. 1987, A&A, 173, 293
Kurucz, R. L. 1979, ApJS, 40, 1
Le Bertre, T., Matsuura, M., Winters, J. M., Murakami, H., Yamamura, I., Freund, M., & Tanaka, M. 2001, A&A, 376, 997
Lee, Y.-W., Demarque, P., & Zinn, R. 1987, in IAU Colloq. 95, The Second Conference on Faint Blue Stars, ed. A. G. D. Phillip, D. S. Hayes, & J. W. Liebert (Schenectady: L. Davis), 137
Lejeune, T., Cuisinier, F., & Buser, R. 1997, A&AS, 125, 229 (LCB97)
Liu, M. C., Charlot, S., & Graham, J. R. 2000, ApJ, 543, 644 (LCG00)
Liu, M. C., Graham, J. R., & Charlot S. 2002, ApJ, 564, 216 (LGC02)
Lorenz, H., Böhm, P., Capaccioli, M., Richter, G.M., & Longo, G. 1993, A&A, 277, L15
Luppino, G. A., & Tonry, J. L. 1993, ApJ, 410, 81
Mei, S., Quinn, P. J., & Silva, D. R. 2001, A&A, 371, 779
Mould, J. R. 2000, ApJ, 529, 786
Neilsen, E. H., & Tsvetanov, Z. I. 2000, ApJ, 536, 255
Origlia, L., & Leitherer, C. 2000, AJ, 119, 2018 (OL00)
Pahre, M. A. 1999, ApJ, 515, 79
Pahre, M. A., & Mould, J. R. 1994, ApJ, 433, 567
Peletier, R. F., Davies, R. L., Illingworth, G. D., Davis, L. E., Cawson, M. 1990, AJ, 100, 1091
Reid, I. N. 1998, in ASP Conf. Ser. 142, The Stellar Initial Mass Function, ed. G. Gilmore & D. Howell (San Francisco: ASP), 121
Reimers, D. 1975, in Problems in Stellar Atmospheres and Envelopes, ed. B. Bascheuk, W. H. Kegel, & G. Traving (Berlin: Springer), 229
Renzini, A. 1981, in IAU Colloq. 59, Effects of Mass Loss on Stellar Evolution, ed. C. Chiosi & R. Stalio (Dordrecht: Reidel), 319
———. 1998, AJ, 115, 2459
Renzini, A., & Buzzoni, A. 1986, in Spectral Evolution of Galaxies, ed. C. Chiosi & A. Renzini (Dordrecht: Reidel), 195
Renzini, A., & Fusi Pecci, F. 1988, ARA&A, 26, 199
Rood, R. T. 1973, ApJ, 184, 815
Saglia, R.P., Maraston, C., Thomas, D., Bender, R., & Colless, M. 2002, ApJ, 579, L13
Salpeter, E. E. 1955, ApJ, 121, 161
Scalo, J. M. 1986, Fundam. Cosmic Phys., 11, 1
Sodemann, M., & Thomsen, B. 1995, AJ, 110, 179
Terlevich, A. I., & Forbes, D. A. 2002, MNRAS, 330, 547 (TF02)
Tonry, J. L., Ajhar, E. A., & Luppino, G. A. 1990, AJ, 100, 1416 (TAL90)
Tonry, J. L., Blakeslee, J. P., Ajhar, E. A., & Dressler, A. 1997, ApJ, 475, 399 (TBAD97)
Tonry, J. L., Dressler, A., Blakeslee, J. P., Ajhar, E. A., Fletcher, A. B., Luppino, G. A., Metzger, M. R., & Moore, C. B. 2001, ApJ, 546, 681 (T01)
Tonry, J. L., & Schechter, P. L. 1990, AJ, 100, 1794
Tonry, J. L., & Schneider, D. P. 1988, AJ, 96, 807 (TS88)
Trager, S. C., Faber, S. M., Worthey, G., & Gonzalez, J. J. 2000, AJ, 120, 165 (TFWG00)
Vassiliadis, E., & Wood, P. R. 1994, ApJS, 92, 125 (VW94)
Weiss, A., Peletier, R. F., & Matteucci, F. 1995, A&A, 296, 73
Worthey, G. 1993, ApJ, 415, L91 (W93)
———. 1994, ApJS, 95, 107